Department of Surgery Oncology and Gastroenterology

PhD course in Clinical and Experimental Oncology and Immunology

XXXI series

Investigation of Metabolic Heterogeneity and Clonal Selection Driven by anti-VEGF therapy in Ovarian Cancer

Coordinator: Prof. Paola Zanovello

Department of Surgery Oncology and Gastroenterology, Padua, Italy

Supervisor: Dr. Stefano Indraccolo

Veneto Institute of Oncology IOV – IRCCS, Padua, Italy

Ph.D. student: Martina Tognon

2017/2018

INDEX

Abstract

The process of neoplastic transformation is associated with profound metabolic changes, including the widely studied dysregulated glucose metabolism. It is also increasingly recognized that tumors are metabolically heterogeneous, including both inter- and intra-tumor metabolic heterogeneity. However, whether this phenomenon depends on the existence of sub-populations endowed with different metabolic features or, rather, local modulation of the metabolism associated with microenvironment factors, such as hypoxia, has less been investigated. Along this line, we recently reported that anti-VEGF therapy (Bevacizumab) induces a stable metabolic change in epithelial ovarian cancer (EOC) xenografts that correlates with resistance to anti-angiogenic therapy.

Aim of this Project is (I) to investigate whether metabolic heterogeneity exists at the clonal level in cancer cells; (II) to investigate the metabolic profile associated with this phenomenon and (III) establish whether anti-angiogenic therapy might shew tumor metabolism, leading to selection of metabolic variants poorly represented in the original tumor (IV) and whether it is possible to treat the resistant cell population with drugs targeting their key metabolic features.

To achieve these aims, we initially isolated by limiting dilution several (n=10-35) clones from established ovarian cancer cell lines previously characterized for their glycolytic activity. Indeed, IGROV-1 and SKOV3 cells are prototypes of poorly glycolytic cells, whereas OC316 cells are highly glycolytic cells. OAW42, A2780 and A2774 ovarian cancer cell lines showed an intermediate glycolytic profile compared to IGROV1 and OC316 cells, according to measurements of glucose consumption and lactate production *in vitro.*

We speculated that highly glycolytic cells could be relatively glucose addicted and hence tolerate less glucose starvation, compared with poorly glycolytic cells. To test this hypothesis, we cultivated clones either in the presence or in the absence of glucose (2 g/l) in the medium. Following 1-2 days in culture, clones were scored by optical microscopy. We used the acronym GDS to refer to a

Glucose Deprivation Sensitive clone or GDR to indicate a clone relatively Resistant to Glucose Deprivation. Results showed that OC316-derived clones were exclusively of the GDS type, whereas IGROV-1 and SKOV3 cancer cell lines included both GDR (55%) and GDS (45%) clones. OAW42 cells were composed by 68% of GDR and 32% of GDS clones, A2780 and A2774 cells showed high enrichment in GDR clones.

The GDR/GDS phenotype was substantially stable when clones were analyzed over separate weeks. Moreover, GDS clones did not express higher levels of transcripts link with glycolysis pathway or elevate lactate production compared with GDR clones. We performed a Seahorse analysis and we observed that Oxigen Consumption Rate was higher in GDR compared to GDS clones. Metabolomic analysis showed that the majority of pathways differentially active in GDS versus GDR clones were linked to mitochondrial functions. Unexpectedly, we could not discriminate GDS clones for their glycolytic activity, but we noticed an altered mitochondria pathway in GDR group compared to GDS clones. We also evaluated the modulation of different pathways in GDR and GDS clones under glucose starvation.

Next, to investigate whether anti-angiogenic therapy would perturb the GDS/GDR ratio, we isolated GDS and GDR clones from *ex vivo* cultures of Control and Bevacizumab-treated IGROV-1 tumors. In the case of clones derived from Control tumors, the percentage of GDR and GDS clones was similar to that found in the parental IGROV-1 cell line. Cultures derived from Bevacizumab-treated tumors had an enrichment in GDR clones, suggesting that anti-VEGF therapy might perturb metabolic heterogeneity in tumors.

Riassunto

Il processo di trasformazione neoplastica è associato ad un profondo cambiamento metabolico che comprende anche l'ampiamente studiata modulazione del metabolismo del glucosio. È inoltre sempre più apprezzato il fatto che i tumori sono metabolicamente eterogenei, compresa l'eterogeneità metabolica intra- e inter-tumorale. Tuttavia, non è ancora stato ampiamente studiato se questo fenomeno dipenda dall'esistenza di sottopopolazioni tumorali dotate di caratteristiche metaboliche diverse oppure da modulazioni locali del metabolismo associato a fattori del microambiente, come per esempio l'ipossia. In base a queste osservazioni, abbiamo recentemente dimostrato che la terapia che prevede l'utilizzo di un anticorpo monoclonale anti-VEGF, Bevacizumab, induce un cambiamento metabolico stabile in xenotrapianti di cancro ovarico epiteliale che correla con un'aumentata aggressività tumorale e la resistenza alla terapia anti-angiogenica.

Lo scopo di questo progetto è quello di indagare se esiste eterogeneità a livello clonale in colture di cellule tumorali e di studiare l'aspetto metabolico associato a questo fenomeno. Abbiamo voluto stabilire se alcune terapie mirate possano modificare il metabolismo tumorale, grazie alla selezione di varianti metaboliche scarsamente rappresentate nel tumore originale e quando sia possibile, trattare queste cellule tumorali con un inibitore diverso dal Bevacizumab.

Per raggiungere questi obiettivi, abbiamo inizialmente isolato, usando diluizioni seriali, diversi cloni (n = 10-35) da linee cellulari di cancro ovarico, precedentemente caratterizzate per la loro attività glicolitica. Infatti, le cellule IGROV-1 e SKOV3 sono prototipi di cellule scarsamente glicolitiche, mentre le cellule OC316 sono altamente glicolitiche. Le linee cellulari di cancro ovarico OAW42, A2780 e A2774 hanno mostrato un profilo glicolitico intermedio rispetto alle cellule IGROV-1 e OC316, in accordo con le misure della produzione di lattato e del consumo del glucosio *in vitro*. Abbiamo ipotizzato che cellule altamente glicolitiche potrebbero essere relativamente dipendenti dal glucosio e quindi

meno tolleranti se nel terreno di coltura manca questo nutriente, rispetto alle cellule scarsamente glicolitiche. Per verificare questa ipotesi, abbiamo coltivato i cloni in presenza o in assenza di glucosio (2 g/l) nel terreno di coltura.

Dopo 72h in cui i cloni sono stati sottoposti a deprivazione di glucosio, sono stati valutati attraverso la microscopia ottica. Abbiamo usato l'acronimo GDS per riferirci ad un clone sensibile alla deprivazione di glucosio e GDR per indicare un clone relativamente resistente alla deprivazione di glucosio. I risultati hanno mostrato che i cloni derivanti dalla coltura cellulare OC316 erano esclusivamente del tipo GDS, mentre nelle linee cellulari IGROV-1 e SKOV3 erano presenti entrambi i due sottogruppi di cloni GDR (55%) e cloni GDS (45%). La linea cellulare OAW42 era composta per il 68% da cloni GDR e per il 32% da cloni GDS, invece le linee A2780 e A2774 hanno mostrato un alto arricchimento nella % di cloni GDR. Il fenotipo GDR/GDS è sostanzialmente stabile anche dopo settimane di analisi. Inoltre, abbiamo osservato che i cloni GDS non esprimono livelli più elevati di trascritti collegati con la via glicolitica e neanche livelli più elevati di produzione di lattato rispetto ai cloni GDR. Abbiamo effettuato un'analisi con la metodica del Seahorse e abbiamo osservato che il tasso di consumo di ossigeno era aumentato nel gruppo dei GDR rispetto ai cloni GDS.

L'analisi metabolomica ha mostrato che la maggior parte delle vie diversamente regolate era legata alla funzione mitocondriale nei cloni GDR. Inaspettatamente, non abbiamo potuto discriminare i cloni GDS per la loro attività glicolitica ma abbiamo notato una possibile alterazione dell'attività mitocondriale nel gruppo dei cloni GDR rispetto ai cloni GDS. Abbiamo anche valutato la modulazione di diverse vie metaboliche nei cloni GDR e GDS in condizioni di deprivazione di glucosio. Successivamente, abbiamo isolato i cloni GDR e GDS da colture cellulari *ex vivo* derivanti da tumori IGROV-1 trattati con Bevacizumab o di controllo. Abbiamo indagato se la terapia anti-angiogenica porta ad un'alterazione del rapporto GDR/GDS. Nel caso dei tumori di controllo, la percentuale dei cloni GDR e GDS isolati, era simile a quella trovata nelle cellule parentali IGROV-1. Le colture cellulari derivate da tumori trattati con Bevacizumab hanno mostrato un

arricchimento nel numero di cloni GDR. Questo può suggerire che la terapia anti-VEGF perturba l'eterogeneità metabolica tumorale.

1.Introduction

1.1 Cancer breaking news

Cancers are defined by the <u>National Cancer Institute (NCI)</u> as a collection of diseases in which abnormal cells can divide and spread to nearby tissue. As this definition suggests, cancers can arise in many parts of the body (leading to a range of cancer types) and in some cases spread to other parts of the body through the blood and lymph systems (*1*).

Cancer is a major public health problem worldwide, making it the second leading cause of death (second only to cardiovascular diseases) in United State.

Figure 1.1 describe the most common cancers expected to occur in men and women in 2018. In men, the 42% of all cancer cases comprises prostate, lung and bronchus and colorectal cancer, with prostate cancer diagnosed 1 in 5 new cases. For women, the three most common cancers are breast, lung and colorectal cancer; breast cancer is 30% all new cancer diagnoses in women (*2*). Lung, prostate and colorectal cancer are the most common causes of cancer death in men the lung, breast and colorectal cancer in women (*2*).

In the United States in 2018 4.700 new diagnoses of cancer and almost 1.700 death of cancer per day will be expected.

Estimated New Cases

	Males			Females		
Prostate	164,690	19%	Breast	266,120	30%
Lung & bronchus	121,680	14%	Lung & bronchus	112,350	13%
Colon & rectum	75,610	9%	Colon & rectum	64,640	7%
Urinary bladder	62,380	7%	Uterine corpus	63,230	7%
Melanoma of the skin	55,150	6%	Thyroid	40,900	5%
Kidney & renal pelvis	42,680	5%	Melanoma of the skin	36,120	4%
Non-Hodgkin lymphoma	41,730	5%	Non-Hodgkin lymphoma	32,950	4%
Oral cavity & pharynx	37,160	4%	Pancreas	26,240	3%
Leukemia	35,030	4%	Leukemia	25,270	3%
Liver & intrahepatic bile duct	30,610	4%	Kidney & renal pelvis	22,660	3%
All Sites	**856,370**	**100%**	**All Sites**	**878,980**	**100%**

Estimated Deaths

	Males			Females		
Lung & bronchus	83,550	26%	Lung & bronchus	70,500	25%
Prostate	29,430	9%	Breast	40,920	14%
Colon & rectum	27,390	8%	Colon & rectum	23,240	8%
Pancreas	23,020	7%	Pancreas	21,310	7%
Liver & intrahepatic bile duct	20,540	6%	Ovary	14,070	5%
Leukemia	14,270	4%	Uterine corpus	11,350	4%
Esophagus	12,850	4%	Leukemia	10,100	4%
Urinary bladder	12,520	4%	Liver & intrahepatic bile duct	9,660	3%
Non-Hodgkin lymphoma	11,510	4%	Non-Hodgkin lymphoma	8,400	3%
Kidney & renal pelvis	10,010	3%	Brain & other nervous system	7,340	3%
All Sites	**323,630**	**100%**	**All Sites**	**286,010**	**100%**

Figure 1.1: Ten leading cancer types for the estimated new cancer cases and deaths by sex, United States, 2018. (2)

The incidence trends from 1999 to 2014 show that the Incidence rates among men decreased throughout the study period, with the decrease accelerating from 0.6% (on average) per year during 1999 to 2008 to 2.2% (on average) per year during 2008 to 2014. In contrast, over the same 15-year period, incidence rates among women were stable (*3*).

In 2016, 8.9 million people are estimated to have died from the various forms of cancer. The Institute for Health Metrics and Evaluation (IHME) put relatively small error margins around this global figure.

Progress against many other causes of deaths and demographic drivers of increasing population size, life expectancy and—particularly in higher-income countries—aging populations mean that the total number of cancer deaths continues to increase. This is a very personal topic to many: nearly everyone knows or has lost someone dear to them from this collection of diseases (*4*).

1.1.1 Hallmarks of cancer

"**The Hallmarks of Cancer**" was published in 2000 in *Cell* journal by Douglas Hanahan and Robert Weinberg (*5*). The authors demonstrated that the complexity of cancer can be reduced to a small number of underlying principles. According to this study, all cancers share six common hallmarks regulating the transformation of normal cells into cancer cells (Figure 1.2).
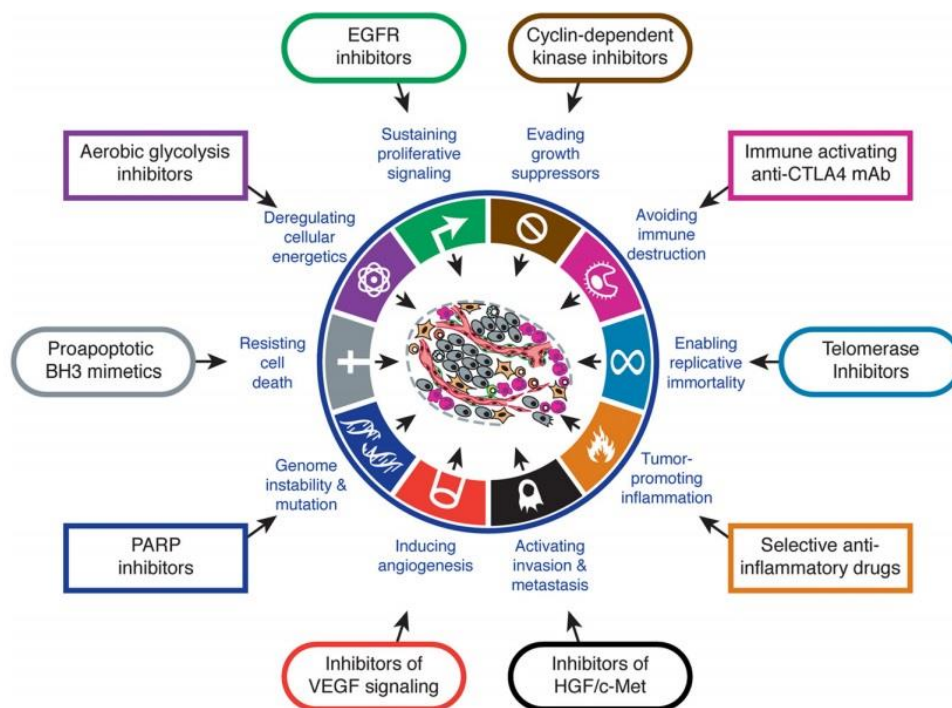

Figure 1.2: The Hallmarks of Cancer: Next Generation (*5*)

Each hallmarks is a consequence of alterations in key pathway regulating cell homeostasis: 1) Cancer cells stimulate their own growth (self-sufficiency in growth signals); 2) They resist inhibitory signals that might otherwise stop their growth (insensitivity to anti-growth signals); 3) They resist their programmed cell

death (evading apoptosis); 4) They can multiply indefinitely (limitless replicative potential); 5) They stimulate the growth of blood vessels to supply nutrients to tumors (sustained angiogenesis); 6) They invade local tissue and spread to distant sites (tissue invasion and metastasis). In an update published in 2011 "Hallmarks of cancer: the next generation", Weinberg and Hanahan proposed four new hallmarks: 7) abnormal metabolic pathways, 8) evading the immune system, 9) genome instability, and 10) inflammation (*6*). Underlying these hallmarks are genome instability, which generates the genetic diversity that expedites their acquisition, and inflammation, which fosters multiple hallmark functions. Conceptual progress in the last decade has added two emerging hallmarks of potential generality to this list; reprogramming of energy metabolism and evading immune destruction. In addition to cancer cells, tumors exhibit another dimension of complexity: they contain a repertoire of recruited, ostensibly normal cells that contribute to the acquisition of hallmark traits by creating the "tumor microenvironment." Recognition of the widespread applicability of these concepts will increasingly affect the development of new means to treat human cancer. Figure 1.2 show all the hallmarks of cancer (old and the emerging) and drugs that interfere with each of the acquired capabilities necessary for tumor growth and progression. Some of these drugs are in clinical trials or, in some cases, are approved for clinical use for the treatment of human cancers. The drugs listed in Figure 1.2 are only few illustrative examples compared to the huge amount of candidate drugs to be tested and possibly targeting molecules involved in cancer hallmark acquisition (*6*).
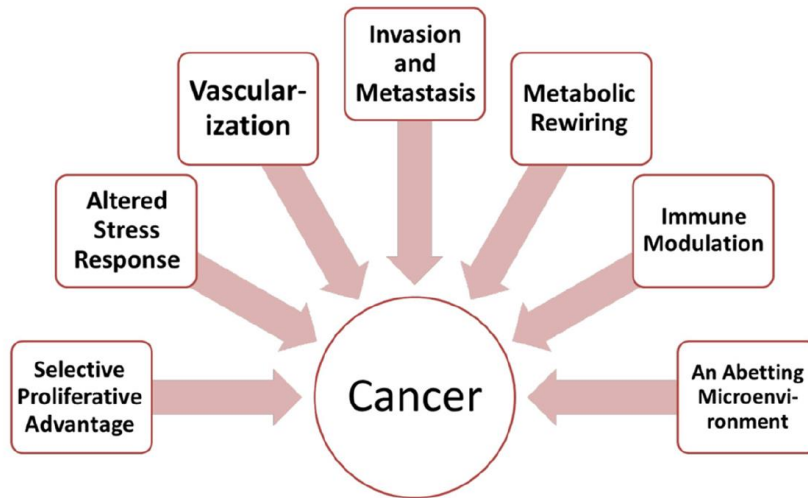
Figure 1.3: Revisiting the hallmarks of cancer (*7*)

A more recent review of cancer hallmarks (*7*) aimed to drawing a more organized and updated pictures of hallmarks (Figure 1.3) organizing previous data according to seven cancer related features: <u>selective growth</u> and <u>proliferative advantage</u>, <u>altered stress response favoring overall survival</u>, <u>vascularization</u>, <u>invasion and metastasis</u>, <u>metabolic rewiring</u>, an <u>abetting microenvironment</u> and <u>immune modulation</u> (*7*).

The idea of the hallmarks is important to keep in mind that cancer is not a single disease but a complex disease involving genetic/epigenetic and environmental factors.

1.2 Ovarian cancer

1.2.1 Anatomy of ovaries

Ovaries are female reproductive glands placed at the sides of the uterus (Figure 1.4) and involved in eggs (ova) production and, thus, reproduction. The eggs travel from the ovaries through the fallopian tubes into the uterus where the fertilized egg settles in and develops into a fetus. The ovaries are also the main source of the female hormones estrogen and progesterone. One ovary is on each side of the uterus.
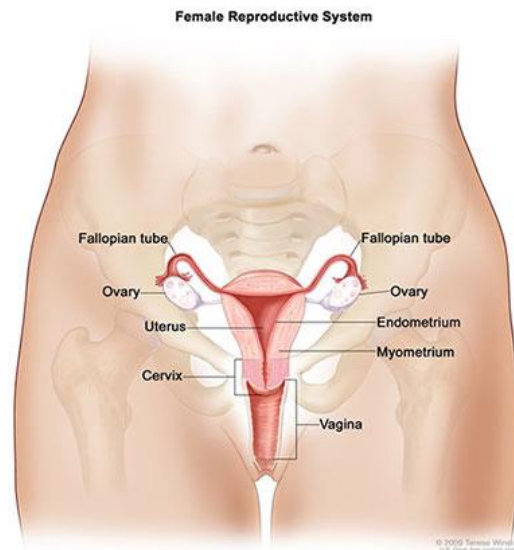
Figure 1.4: Reproductive System, Female, Anatomy. Source: Terese Winslow (Illustrator), National Cancer Institute (*8*).

The ovaries are mainly made up of three kinds of cells. Each type of cell can develop into a different type of tumor:

- Epithelial tumors start from the cells that cover the outer surface of the ovary. Most ovarian tumors are epithelial tumors.
- Germ cell tumors start from the cells that produce the eggs (ova).
- Stromal tumors start from structural tissue cells holding the ovary together and producing the female hormones estrogen and progesterone.

Some of these tumors are benign (non-cancerous) and never spread beyond the ovary. Malignant (cancerous) or borderline (low malignant potential) ovarian tumors can spread (metastasize) to other parts of the body and can be fatal (*9*).

1.2.2 Epidemiology, risk and genetic in ovarian cancer

In 2018, approximately 22.240 new cases of ovarian cancer diagnosed and 14.070 related deaths have been estimated only in United States (*10*). Unfortunately, ovarian cancer is characterized by very mild symptoms, leading to

a late stage diagnoses in most of the cases. Indeed, symptoms, even if present, are vague and are easily attributed to common uro-genital, gynecological or gastro-intestinal pathologies (*11*). The most common sign of advanced disease is ascites that cause swelling of the abdomen(*12*). For this reason, ovarian cancer has a low survival rates and represents the 5% of female cancer death (Figure 1.1). However, the early detection, made by prevention, allows to increase the 5-years relative survival rate to 93% (*10*).

A family history of breast or ovarian cancer strongly enhances the risk to develop ovarian cancer (*13*). The risk of developing invasive ovarian cancer is 50% in women who have a first-degree relative with a history of ovarian cancer and 10% in women who have a first-degree relative with breast cancer (*14*). Multiple factors may increase the risk of developing ovarian cancer, including hereditary factors, such as germinal mutations in the two tumor suppressors *BRCA1* or *BRCA2*. *BRCA1* mutations are associated with a 50% to 80% probability of developing breast cancer and a predisposition to ovarian cancer (*11, 15*).

1.2.3 Type and stages of ovarian cancer

According to the anatomical district from which the tumor originates, we can distinguish three main categories of ovarian carcinoma: <u>epithelial</u>, if it originates from epithelial cells of the ovary (about 90% of cases), <u>germline,</u> if it originates from germ cells (about 5% of cases) and <u>stromal</u>, if it originates from ovarian stroma cells (about 5% of cases) (*16*). Five main histological subtypes of ovarian carcinoma can be identified. Each subtype is characterized by distinct clinical features: high-grade serous ovarian cancer (High-Grade Serous, HGSC)(i), low-grade serous (Low-Grade Serous, LGSC)(ii), endometrioid (ENOC, with clear cells (Clear Cell, CCOC))(iii) and mucinous (iv) (*17*). *High-grade serous* subtype is the most common ovarian cancer, which accounts for 70% of the diagnosed invasive ovarian carcinomas. It is usually diagnosed at late stages and, although initially presenting a clear response to chemotherapy, it often develops resistance and leads to death (*17*). Tumor staging can be performed evaluating the size of the

tumor mass, the location, the tumor cells lymph nodes infiltration and the presence of distant metastases, it is possible to perform a staging of the tumor. In addition to the TNM (TNM Classification of Malignant Tumours) system, ovarian carcinoma staging can be determined by FIGO (International Federation of Gynecology and Obstetrics) system, which classifies ovarian cancer in four stages (*18*):

-Stage I: the tumor is limited to one or both ovaries, with the possibility of expansion up to the surface of the ovary and the presence of tumor cells in the peritoneal   fluid.

- Stage II: the tumor involves one or both ovaries and extends to the pelvis, i.e. the lower region of the abdomen. Tumor cells may also be found in the peritoneal   fluid.

- Stage III: the tumor involves one or both ovaries. Extrapelvic peritoneal metastases and / or regional lymph nodes are found, ie in the lymph nodes located   in   the   same   area   of   the   primary   tumor.

- Stage IV: presence of metastases in regions distant from both the ovaries and the   peritoneum.

In addition to the stage, the tumor degree is fundamental for the choice of therapeutic strategy. This parameter indicates how much cancer cells differ from those of healthy tissue and gives an idea of the rate of tumor development. By histological analysis of tumor tissue section, the following degrees can be distinguished:

 - Low Grade: tumor cells are very similar to healthy ovarian tissue cells, grow slowly and usually do not spread into the surrounding tissue.

- Intermediate Degree: Tumor cells are different from healthy tissue cells, but have not invaded surrounding tissues.

- High Degree: cells have an abnormal appearance, grow rapidly and have a high probability of spreading into surrounding tissues and blood. The higher the stage and the degree of the tumor, the worse patient's prognosis.

1.2.4 Ovarian cancer treatment

Standard therapy for ovarian cancer involves surgical maximal reduction of tumor volume, followed by chemotherapy or radiotherapy. Combinations of different chemotherapeutics are used for the different subtypes of ovarian carcinoma. For example, serous tumors seem to respond better to therapy by combining paclitaxel and cisplatin, whereas clear cell tumors seem to respond better to the combination of irinotecan plus cisplatin (REF). However, despite the presence of an initial response, tumor eventually develops chemotherapy resistance.

Here the standard therapies used to ovarian cancer treatment:

-***Radiation therapy*** uses high energy x-rays or particles to kill cancer cells. These x-rays may be given in a procedure that is much like having a regular x-ray. Aggressive chemotherapy is usually more effective, so radiation therapy is rarely used in this country as the main treatment for ovarian cancer. However, it can be useful in treating areas where the cancer has spread, either near the main tumor or in a distant organ, like the brain or spinal cord.

By external radiation therapy a machine focuses the radiation on the area affected by the cancer. The procedure itself is painless. Each treatment lasts only a few minutes, but the setup time usually takes longer (*19, 20*).

-**Chemotherapy** (chemo) is the use of drugs to treat cancer. Most often, chemo is a systemic treatment, meaning the drugs enter the bloodstream and reach almost all areas of the body. Chemo can be useful to kill very small amounts of cancer cells that may still be around after surgery, for cancers that have metastasized (spread), or to shrink very large tumors to make surgery easier. Most of the time, chemo uses drugs that are injected into a vein (IV) or given by mouth. In some cases, chemotherapy may also be injected through a catheter (thin tube) directly into the abdominal cavity. This is called *intraperitoneal (IP) chemotherapy*. Chemo for ovarian cancer usually involves getting two different types of drugs together. Getting a combination of drugs instead of just one drug alone seems to work better as a first treatment for ovarian cancer. Usually, the

combination includes a type of chemo drug called a *platinum compound* (usually cisplatin or carboplatin), and another type of chemo drug called a *taxane*, such as paclitaxel (Taxol®) or docetaxel (Taxotere®). These drugs are usually given as an IV (put into a vein) every 3 to 4 weeks (*21-23*).

-Targeted therapy is a type of cancer treatment that uses drugs or other substances to identify and attack cancer cells while doing little damage to normal cells. These therapies attack the cancer cells' inner workings – the programming that makes them different from normal, healthy cells. Each type of targeted therapy works differently, but they all change the way a cancer cell grows, divides, repairs itself, or interacts with other cells.

Bevacizumab (Avastin) belongs to a class of drugs called *angiogenesis inhibitors*. For cancers to grow and spread, they need to make new blood vessels to nourish themselves (called angiogenesis). This drug attaches to a protein called VEGF (that signals new blood vessels to form) and slows or stops cancer growth (*24, 25*).

Olaparib (Lynparza), rucaparib (Rubraca), and niraparib (Zejula) are drugs known as a *PARP (poly(ADP)-ribose polymerase) inhibitors*. PARP enzymes are normally involved in one pathway to help repair damaged DNA inside cells. The *BRCA* genes (*BRCA1* and *BRCA2*) are also normally involved in a different pathway of DNA repair, and mutations in those genes can block that pathway. By blocking the PARP pathway, these drugs make it very hard for tumor cells with a mutated *BRCA* gene to repair damaged DNA, which often leads to the death of these cells (*26, 27*).

1.3 Angiogenesis as a pathological process

Angiogenesis is a tightly regulated biological process through which new blood vessels are generated from pre-existing ones. This is distinct from vasculogenesis, which is the *de novo* formation of endothelial cells from mesoderm cell precursors (*28*). The angiogenesis is modulated by different

angiogenic factors such as the **vascular endothelial growth factor** (**VEGF**) (Figure 1.5). Angiogenesis is regulated by the equilibrium from factors that can promote (pro-angiogenic) or other factors that inhibit (anti-angiogenic) this critical process. In particular, angiogenesis is activated when pro-angiogenic factors become prevalent (angiogenic switch).

Angiogenesis, as a pathological process, plays an essential role in the formation of a new vascular network to supply nutrients, oxygen and immune cells to the cancer. Hence, targeting angiogenesis might plausibly reduce intra-tumoral levels of oxygen and nutrients resulting in tumor starvation and thus in reduced tumor growth (*29*). Judah Folkman and colleagues' vision of targeting the tumor neovasculature as a new modality of cancer therapeutics has inspired a series of drugs that inhibit VEGF signaling with different mechanisms of action (*30, 31*) with associated beneficial responses, representing proof of principle and new additions to the armamentarium of anti-cancer drugs.
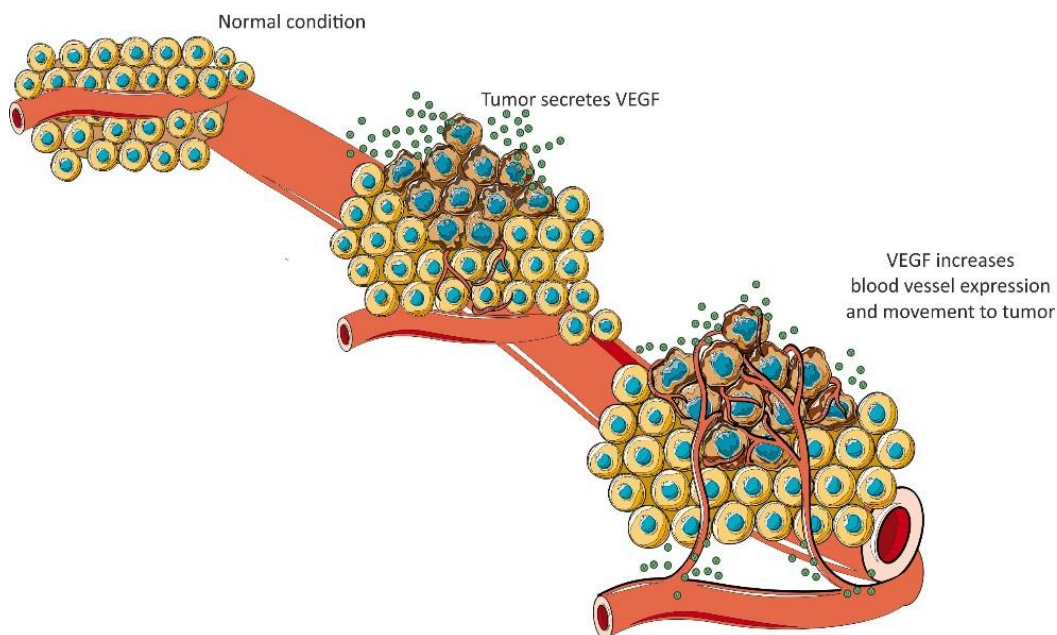

Figure 1.5. Angiogenesis process regulated by VEGF.

1.3.1 Anti-angiogenic therapies and mechanisms of resistance

Anti-angiogenic therapies have been rapidly translated with great expectations from preclinical cancer models to clinical practice (*32-35*). However, similarly to many other targeted therapies, clinical responses to angiogenesis inhibitors (AI) are typically limited, manifested as increased, progression-free survival (PFS) without a significant impact on overall survival (OS) (*36, 37*). Indeed, patients present survival benefit in the range of months but generally OS is often not prolonged and no permanent cure is observed for renal cell carcinoma (RCC) (*38, 39*), breast (*40*) and colon cancer (*41*). Concurrent with such clinical investigations, different preclinical studies of AI in various mouse models of human cancer have revealed multiple forms of adaptive resistance that enable tumors to evade the effects of AI therapy (*30, 36, 42-45*) . In these works, they have described several different mechanisms of resistance to anti-angiogenic therapies. One of these suggested that tumors may activate alternative pro-angiogenic signals that promote revascularization and facilitate tumor regrowth. O. Casanovas et al demonstrated in a model of renal cell carcinoma (RCC) that the inhibition of VEGFR2 (MAb DC101) is effective for a limited period. Indeed, he observed resistance development caused by hypoxia-triggered upregulation of other proangiogenic factors (FGFs and Ephrins) that restimulate tumor angiogenesis in a VEGF-independent manner. Moreover, he promoted a double treatment to block both VEGFR2 and FGF ligands as a possible mechanism to overcome the resistance associated with the revascularization. Apart from vascular resistance, due to bypassing of VEGF blockade by proangiogenic factors produced by either tumor cells, stromal cells or various types of bone marrow-derived cells, resistance has also been associated with selection of clones resistant to hypoxia, and acquisition of an invasive phenotype (*36, 42, 46, 47*).

One mechanism of resistance to anti-angiogenic therapy is associated with induction of stably glycolytic phenotype (*48, 49*). In our laboratory, published data (*49*) demonstrated that anti-VEGF therapy with Bevacizumab stably modulates the glycolytic phenotype in ovarian cancer models. Bevacizumab is a

recombinant humanized monoclonal IgG1 antibody that targets vascular endothelial growth factor-A. In 2012, Bevacizumab has been approved for the treatment of epithelial ovarian cancer (EOC), both as single-agent drug and in combination with cytotoxic chemotherapy. However, the mechanism to underlying metabolic modifications leading to resistance remains unclear. We hypothesized this stable metabolic modification could be due to either selection of a pre-existing subpopulation of highly glycolytic tumor cells or, alternatively, be accounted for by epigenetic reprogramming of cell metabolism.

Recently, metabolic symbiosis has been described in several mouse models of cancer in response to potent angiogenesis inhibitors (*50, 51*). Metabolic symbiosis is considered a particular form of adaptation to hypoxia. In particular, two recent Cell Reports presented by *E. Allen et al* and *L. Pisarsky et al* described two possible mechanism to overcome the resistance associated with antiangiogenic therapy. However, there has not been confirmatory assessment in the clinical setting with human patient samples (*52, 53*).

1.4 Metabolism and cancer

Cancer metabolism has received a substantial amount of interest over the past decade (*54*). The first study which affirmed the role of metabolism in carcinogenesis is described by the German physiologist Otto Warburg, who in the 1920s, demonstrated that cancer cells - at variance with normal cells - rely on glycolysis instead of mitochondrial oxidative phosphorylation (OXPHOS) to produce ATP even under aerobic conditions (*55*). Warburg originally hypothesized that the glycolytic switch in cancer cells was a consequence of defects in mitochondria, which impair aerobic respiration. Currently, however, it is known that mitochondria are not damaged in the most cancer cells, suggesting that aerobic glycolysis essentially represents an adaptive choice of tumours (*56*).

1.4.1 Core metabolic pathways and enzymes in cancer cells

In cancer cells, the canonical energy metabolism pathways are often truncated (glycolysis, tricarboxylic acid (TCA) cycle) or redirected (glutaminolysis or serine and lipid biosynthesis) (Figure 1.6). Briefly, glucose enters into cancer cells through glucose transporters and is phosphorylated to glucose-6-phosphate (G6P) by an irreversible reaction catalyzed by the hexokinase. G6P either proceeds through glycolysis to produce pyruvate or through the pentose phosphate pathway (PPP) to generate ribose-5-phosphate and NADPH. The PPP is connected at the first step of glycolysis starting with G6P dehydrogenase (G6PD) and has both an oxidative and nonoxidative arm. G6P oxidation produces the reducing equivalents, in the form of NADPH, important cellular antioxidant, and cofactor for fatty acid biosynthesis. Moreover, the PPP provides cancer cells with pentose sugars for the biosynthesis of nucleic acids. The first enzymes involved in the nonoxidative arm of the PPP are transaldolase (TA) and transketolase (TKT). Ribose-5-phosphate and xylulose-5-phosphate, generated by the oxidative PPP, can be further metabolized into fructose-6-phosphate (F6P) and glyceraldehyde-3-phosphate (G3P) to reenter into glycolysis for ATP production, depending on the cell requirement. Thus, the PPP plays a key role in cancer cells to supply their anabolic demands and to counteract oxidative stress. The serine pathway is branched to glycolysis *via* 3-phosphoglycerate (3PG), which is converted by phosphoglycerate dehydrogenase (PHGDH) into phosphohydroxypyruvate (P-PYR). This pathway produces serine and glycine, essential precursors for synthesis of proteins and nucleic acids through the folate cycle. Following glycolysis, pyruvate is either converted into lactate by lactate dehydrogenase A (LDHA) and released through monocarboxylate transporters, MCT4 and MCT1, further causing extra cellular acidification, or converted into acetyl-CoA, through the pyruvate dehydrogenase (PDH) complex. Acetyl-CoA enters into TCA cycle and produces ATP, NADH, and FADH2 molecules. Reduced cofactors are then oxidized by the electron transport chain (ETC) complexes for ATP production. Glutamine and other amino acids can also replenish the TCA

cycle. Indeed, the first step of glutaminolysis is the conversion of glutamine into glutamate by the glutaminase (GLS). Glutamate is subsequently converted into alpha-ketoglutarate (αKG) that fuels back the TCA cycle. Fatty acid degradation can also supply the TCA cycle through beta-oxidation, which produces acetyl-CoA. Reciprocally, citrate, a TCA cycle intermediate, can be used as a precursor for fatty acid synthesis and for NADPH production through the ATP citrate lyase (ACL). Citrate is subsequently converted to acetyl-CoA and oxaloacetate (OAA) into the cytoplasm. Acetyl-CoA is used for fatty acid synthesis through its conversion to malonyl-CoA by acetyl-CoA carboxylase (ACC) and to palmitic acid by the fatty acid synthase (FASN). OAA is converted to malate, which is then decarboxylated into pyruvate, by the malic enzyme (ME1) and produces NADPH.
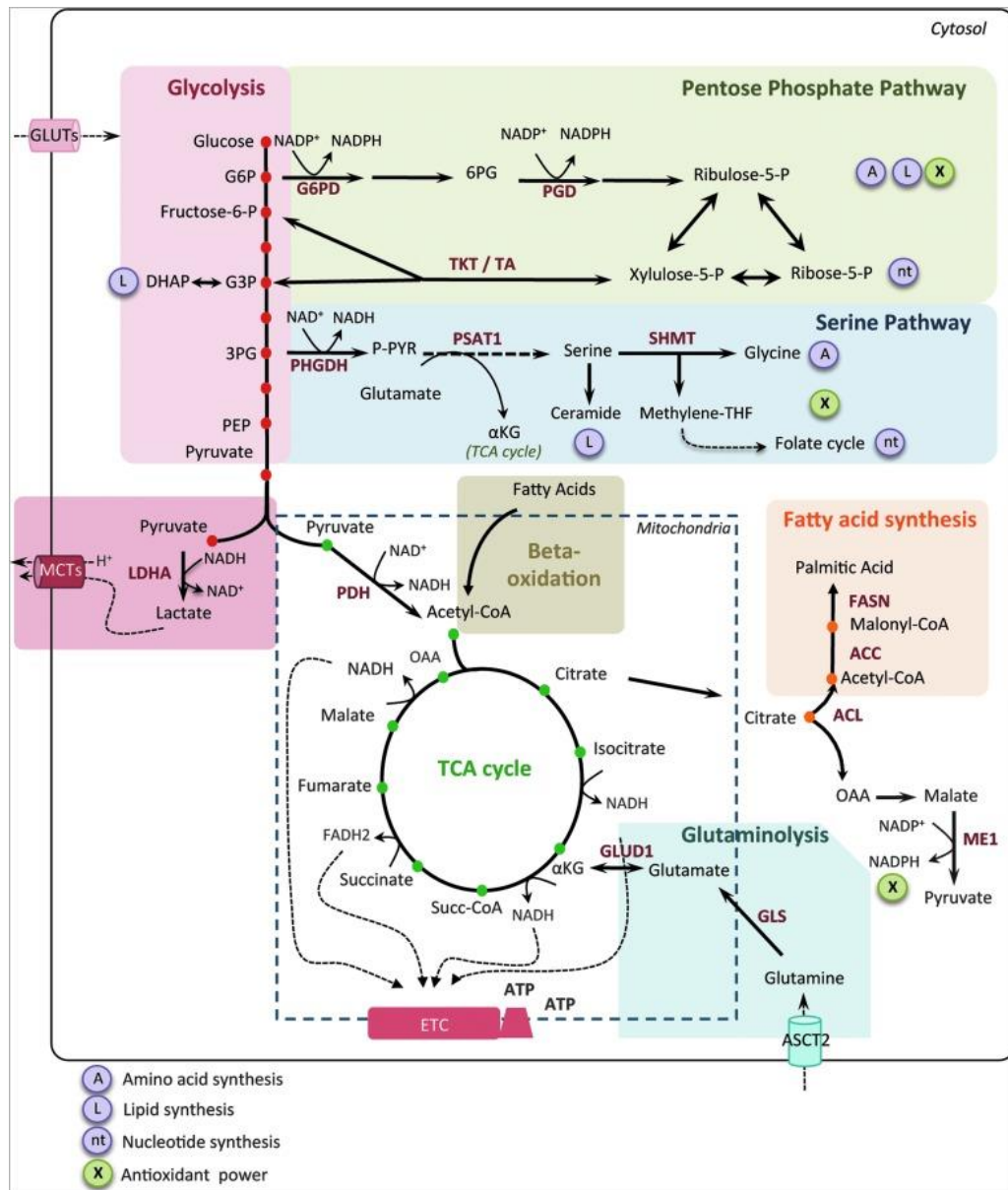
Figure 1.6. Signaling pathways that regulate cancer metabolism (53). Mitochondria are represented by *dotted line*. ACC, acetyl-CoA carboxylase; ACL, ATP citrate lyase; αKG, alpha-ketoglutarate; ASCT2, amino acid transporter; ATP, adenosine triphosphate; DHAP, dihydroxyacetone phosphate; ETC, electron transport chain; FAD, flavin adenine dinucleotide; FASN, fatty acid synthase; F6P, fructose-6-phosphate; GADP, glyceraldehyde-3-phosphate; G3P, glyceraldehyde-3-phosphate; GLS, glutaminase; G6P, glucose-6-phosphate; GLUT, glucose transporter; LDHA, lactate dehydrogenase A; MCT, monocarboxylate transporter; ME1, malic enzyme; NAD, nicotinamide adenine dinucleotide; NADPH, nicotinamide adenine dinucleotide phosphate; OAA, oxaloacetate; PDH, pyruvate dehydrogenase; PEP, phospho-enol-pyruvate; 6PG, 6-phospho-

gluconolactone; 3PG, 3-phopho-glycerate; PGD, phosphogluconate dehydrogenase; PHGDH, phosphoglycerate dehydrogenase; PPP, pentose phosphate pathway; P-PYR, phosphohydroxypyruvate; PSAT1, phosphoserine aminotransferase; SHMT1, serine hydroxymethyl transferase; Succ-CoA, succinyl-CoA; TCA, tricarboxylic acid; TA, transaldolase; TKT, transketolase (*57*).

1.4.2 The metabolic heterogeneity and the concept of clones

The existence of clonal heterogeneity has been documented for a variety of malignancies, but due to multiple technical challenges. The available data are mostly fragmentary, with the extent of clonal heterogeneity and the dependence of clonal heterogeneity on tumor type, subtype, and disease stage remaining mostly unexplored (*58*). Clone is a key concept for our current understanding of tumor biology and comprises both clonal origin and expansions, which contribute to both tumor initiation and promotion (*59, 60*).

Cancer exists in a variety of taxonomically, classes, genera, species, characterized by divergent cells of origin and mutational spectra. Cancers acquire, via mutational and epigenetic changes, a variety of critical phenotype traits that compound to empower territorial expansion, via proliferative self-renewal, migration and invasion; properties that are part and parcel of normal developmental, physiological and repair processes (*61*). Each cancer is individually unique and frequently displays substantial intra-tumor heterogeneity in virtually all distinguishable phenotypic features, such as cellular morphology, tumor histology; gene expression, metabolism, growth rate, and metastatic ability and sensitivity to therapeutic agents.

Since 1980, the tumor heterogeneity was largely studied. Subpopulations have been isolated from cancer of every major histological type and organ site and from both experimental and human cancer. They have been isolated from tumor induced by chemical, physical or viral agents; from long term cell lines; and from tumors of recent origin (*62*). Some published data speculated that cancer "stem cell theory" could explain the origins of heterogeneity, tumor growth is driven by

a rare subpopulation of cells, designated cancer stem cells (CSC) (*63-66*); other reports might argue that genomic/genetic instability drives diversification of cancers (*67-70*). Discussion of the heterogeneity in tumors often concerns the concepts of clones (*70*).

1.4.2.1 Causes of intratumoral heterogeneity

1.4.2.1.1 Genomic instability

According to certain theories, tumorigenesis is reliant on an elevated spontaneous mutation rate (*71*). Notably, in some tumors, including brain tumors, genomic instability results from chromosome-level changes that lead to gains or losses of whole-genome segments, rather than point mutations. This process, termed chromosomal instability, arises from segregation errors that occur during cell division, which might promote genetic diversity by upsetting the balance between activation of oncogenes and tumor suppressors.

1.4.2.1.2 The clonal evolution/selection hypothesis

Evidence of ongoing genomic instability within certain regions of individual tumors and across different metastatic sites, in addition to the existence of these events at the subclonal level, suggests that increased levels of genomic instability promote the emergence of more-competitive subclones. Excessive levels of genomic instability can, however, have adverse effects on cancer cell survival and fitness (*71*). Tumors are likely to require more than just genomic instability alone in order to maintain heterogeneity. Various models have been proposed to explain how clonal diversity is generated and maintained. Although the majority of contemporary studies continue to use the clonal evolution and/or selection framework model. In 1976 Peter Nowell published a landmark perspective on cancer as an evolutionary process, driven by stepwise, somatic cell mutations with sequential, sub-clonal selection (*72*). The implicit parallel was to Darwinian natural selection with cancer equivalent to an asexually reproducing, unicellular,

quasi-species. The modern era of cancer biology and genomics has validated the fundamentals of cancer as a complex, Darwinian, adaptive system (*73, 74*).

The clonal heterogeneity was largely discuss but what characterize the clones population remains undiscovered. We aim to investigate if this heterogeneity exists at clonal level and what characterized the clones population.

1.4.3 Cancer cells sensitivity to glucose starvation

In 2014 K. Birsoy et al (*75*), and A. Pastò et al (*76*) in 2016, published two studies that investigated the glucose starvation response in 28 patient-derived cancer cell lines and in EOC ascitic effusions from 47 carbonplatin-treated patients. In the first study, authors performed a continuous flow culture apparatus (Nutrostat) for maintaining proliferating cells in low nutrient media for long periods of time and then they started with the analysis. They also used several cell lines sensitive or resistant to glucose limitation. The low glucose sensitive cell lines up regulated Oxygen Consumption Rate less than resistant one. They considered two explanations for why low glucose sensitive lines do not increase Oxygen Consumption Rate upon glucose limitation. The data identify a defect in glucose utilization that limits substrates for mitochondria and defect in OXPHOS pathway. In the second work the tumor cells from epithelial ovarian cancer (EOC) patients can be categorized into glucose deprivation-sensitive (GA) and glucose deprivation-resistant (GNA). Their data showed a more pronounced Warburg effect in GA samples, which were significantly enriched in platinum (PLT)-sensitive patients. GA cells presented higher *in vitro* sensitivity to PLT, which could be in part explained by a higher proliferation rate as well as a more active glycolytic machinery. On the other hand, the low glycolytic metabolism of GNA samples was counterbalanced by their higher basal autophagy activity.

These findings suggested that exists a different response to nutrient starvation in cancer cell lines and tumor cells from patients. To better characterized these observations, we tried to decrease the intra-tumor heterogeneity by the study of clones derived from ovarian cancer cell lines. We also investigated if the

presence of a resistant clones subpopulation could be involved in the anti-VEGF

therapy resistance.

2. AIM

During my PhD I investigated whether metabolic heterogeneity exists at the clonal level in cancer cells. We aimed to study metabolic differences between Glucose Deprivation Resistant (GDR) and Glucose Deprivation Sensitive (GDS) clones in ovarian cancer cell lines previously characterized by their glycolytic activity. We studied metabolic heterogeneity at clonal level in vitro and then sought to investigate whether anti-angiogenic therapies might skew tumor metabolism, leading to selection of clones poorly represented in the original tumor. Finally, we tried to identify compounds that target the dis-regulated metabolism selected by Bevacizumab in tumors and may be used to prevent the emergence of resistance to the anti-VEGF therapy.

3. Materials and Methods

3.1 Inhibitors

In this study, the following inhibitors were used:

Lonidamine (MW. 321.16 g/mol**,** Molekula Balliol Business Park, Newcastle Upon Tyne, UK), an MCTs inhibitor, was purchased in powder and resuspended in DMSO

Metformin (MW.165.62 g/mol, Sigma-Aldrich, St. Louis, Missouri, US) a respiratory chain complex I inhibitor, was purchased in powder and resuspended in H_2O milli Q.

3.2 Cell lines and in vitro culture conditions

In this work, we used different cancer cell lines:

- **IGROV-1**, were purchased from ATCC

- **OC316** cells were provided by S. Ferrini (IST, Genoa, Italy)

- **OVCAR3** and **SKOV-3** cells were provided by S. Canevari (IRCCS-INT, Milan, Italy)

- **A2774**, **A2780** and **OAW42** were provided by P. Alberti (IRCCS-INT, Milan, Italy)

OAW42 cell line was cultured in EMEM (Eagle's Minimum Essential Medium, ATCC 30-2003) supplemented with 10% FBS (Fetal Bovine Serum, Life technologies, Paisley, UK) and 2mM L-glutamine (Lonza, Basel, Switzerland). All ovarian cancer cell lines were cultured in RPMI 1640 (EuroClone, Milan, Italy) supplemented with 10% (or 20% in the case of OVCAR3 cells) FBS, 10mM HEPES (Cambrex Bioscience, East Rutherford, NJ), 1% Sodium Pyruvate (Lonza, Basel, Switzerland), 2 mM L-glutamine and 1% of antibiotic-antimycotic mix (Life

Technologies, Paisley, UK). At the indicated time points, cells were harvested and processed for assessment of cell viability, and RNA and protein extraction. The cultures were routinely maintained at 37°C in a humidified 5% CO2/95% air atmosphere

3.3 DNA extraction and quantification

DNA was extracted from cell culture by using the QIAamp DNA mini extraction kit (Qiagen, Hilden, Germany, http://www.qiagen.com) according to the manufacturer's instructions.

For DNA quantification, Qubit assay was used and the DNA concentration was measured by using the Invitrogen Qubit 4 Fluorometer.

3.4 STR analysis

STR (short tandem repeat) loci consist of short, repetitive sequence elements 3-7 base pairs in length. These repeats are well distributed throughout the human genome and are a rich source of highly polymorphic markers, which may be detected using the polymerase chain reaction. Alleles of STR loci are differentiated by the number of copies of the repeat sequence contained within the amplified region and are distinguished from one another using fluorescence detection following electrophoretic separation.

We used the PowerPlex 16 HS System (Promega Corporation, Madison USA) to authenticate cell lines. The system allows co-amplification and three-color detection of sixteen loci (fifteen STR loci and Amelogenin), including Penta E, D18S51, D21S11, TH01, D3S1358, FGA, TPOX, D8S1179, vWA, amelogenin, Penta D, CSF1PO, D12S539, D7S820, D13S317 and D5S818.

The detection of amplified fragments was performed using ABI PRISM 3730xL DNA Analyzer with data collection software 3730 series 4 and analysis of fragments using Gene Mapper 5 software.

We performed STR analysis according to protocol instruction provided by Promega Corporation.

3.5 Generation of GDR and GDS clones

The cloning by limiting dilution methodology describes a procedure to obtain a monoclonal cell population starting from a polyclonal mass of cells. We isolated several clones from different ovarian cancer cell lines (n=20/35 clones/cell culture).

From the parental cultures, we prepared serial dilutions in order to obtain 20 viable cells/ml suspension.

We dispensed the final suspension into 96-well plate in order to obtain 2, 1, 0.5 cells per well.

When a single clone grew up in 96-well plate, we created a clone culture. We did not consider wells there were two or more clones.

In order to expand the single-clone culture we trypsinezed the single clone and we plated it in 2ml of medium in a 24-well plate; from each well, we took 200 ul and we plated twice in a new 96-well plate. After few days,

we changed the medium: for each couple of single-clone we cultured one in the presence of glucose (2g/L) and the other one in the absence of glucose.

We evaluated the resistance to glucose starvation of each clones. Clones were then scored by optical microscopy and we used the acronym GDS to refer to a Glucose Deprivation Sensitive clone or GDR to indicate a clone relatively Resistant to Glucose Deprivation.

Subsequently, we cultured all clones in standard condition in T75 flask.

3.6 Optical Microscopy Analysis

To evaluate the sensibility to glucose starvation of clones, we used Leica optical Microscopy with Leica Application Suite–LAS EZ to take a representative photo about GDR and GDS clones.

3.7 Concentration Measurement of Glucose and Lactate in the Medium

To characterize the glycolytic metabolism of each culture cell lines we plated $2 \cdot 10^5$ cells per well in 6-multi wells tissue culture plates and incubated under normoxic conditions. After 48h supernatants was harvested and centrifugated for 10 minutes at 3000g and then 1mL was analyzed considering the basal values present in the medium. Glucose and lactate concentrations in supernatants were determined by colorimetric methods on an automated analyzer (Dimension RxL, Dade Behring, Milan, Italy). Values were normalized to cells number at the end of the incubation period.

3.8 RNA extraction, reverse transcription PCR (RT-PCR), quantitative RT-PCR (qRT-PCR)

Total RNA was extracted from cells following the Trizol® protocol (Life Technologies), according to the manufacturer's instruction. RNA concentration was determined using NanoDrop ONE (Thermo Scientific,).The instrument provided the sample concentration in ng/µl and the absorbance of the sample at 260nm and 280nm. The ratio (260/280) ranging from 1.8 to 2.1 indicated good quality of RNA (ratio < 1.8 means protein contamination and ratio > 2.1 RNA degradation and truncated transcripts).

cDNA was synthesized from 1 μg of total RNA using the "High Capacity RNA-to-cDNA™ Kit"(Applied Biosystems). Reverse transcription was followed by quantitative PCR using SYBR Green. mRNA PCRs were performed in an ABI Prism 7900HT Sequence Detection System. All reagents were obtained from Life Technologies. Results were analysed using the ΔΔCt method with normalization against β2-microglobulin expression. Primers used for q RT-PCR analysis were:

Gene	Forward primer	Reverse primer
LDH-B	5'-CACCAGTTGCGGAAGAAGA -3'	5'-CAGCCAGAGACTTTCCCAGA -3'
LDH-A	5' -GATTCAGCCCGATTCCGTTAC -3'	5' -ACTCCATACAGGCACACTGG -3'
HKII	5'-GAAGATGCTGCCCACCTTTG-3'	5'-CACCCAAAGCACACGGAAGT-3'
GLUT-1	5'-GATGATGCGGGAGAAGAAGG-3'	5'-AAGACAGCGTTGATGCCAGAC-3'
MCT-1	5'-TGTTGTTGCAAATGGAGTGT-3'	5'-AAGTCGATAATTGATGCCCATGCCAA-3'
MCT-4	5'-GTTGGGTTTGGCACTCAACT-3'	5'-GAAGACAGGGCTACCTGCTG-3'
β2micro	5'-TGCTGTCTCCATGTTTGATGTATCT-3'	5'-TCTCTGCTCCCCACCTCTAAGT-3'

3.9 Seahorse analysis: Oxygen Consumption and Extracellular Acidification Rate

The Seahorse XF24 Extracellular Flux Analyzer (Seahorse Bioscience, San Jose, CA) is an instrument that measures two parameters: the Oxygen Consumption Rate (OCR) and the Extracellular Acidification Rate (ECAR).

We plated 2.5×10^4 cells per well (for each experiment we set up 5 replicates for sample) in RPMI medium supplemented with 10% FBS. The next day, cells were placed in a running DMEM medium (supplemented with 25 mmol/L D-glucose, 2 mmol/L glutamine, 1 mmol/L sodium pyruvate, and without serum and bicarbonate) and preincubated for 30 minutes at 37°C in atmospheric CO2 before starting metabolic measurements.

The cartridge of the instrument was loaded to dispense four different metabolic inhibitors at 20 min intervals: olygomycin (1µM), followed by carbonyl cyanide p trifluoromethoxyphenylhydrazone, FCCP (0.4 µM), antimycin (1µM) and rotenone (1µM; all from Sigma Aldrich) over 2h. Some analysis to measure only ECAR were performed initially depriving glucose to cells and after adding glucose, oligomycin, 2-deoxyglucose (2-DG) and finally the medium. At the end of the experiment, OCR and ECAR values were normalized for the protein content of each sample. Accurate titration with the uncoupler FCCP was performed for each cell type, to utilize the FCCP concentration (400 nmol/L) that maximally increases OCR without being toxic.

3.10 Single Cell analysis technique

In collaboration with Dr.Fabio Del Ben and Dr.ssa Giulia Brisotto (CRO- Aviano (PN), Italy) we performed a single cell analysis to evaluate the secretion of acid from individual living tumor cells. We evaluated two GDR and two GDS clones. The key of this methodology is splitting the cells into small (picoliter/nanoliter) aqueous droplets in oil (making a water-in-oil emulsion) using microfluidic technology. Each droplet contains at most a single cell and molecules secreted by this single cell are retained by the droplet. The pH range of cancer extracellular environment is known to be 6.2-6,9 compared with 7.3-7.4 in normal tissue, and the secretion rate of lactic acid by tumor cells is in the range of 10^{-16} mol cell $^{-1}$ sec $^{-1}$. To screen droplets with higher throughput in a semi-automated way, we engineered an inverted microscope, so that each droplet can be analyzed using laser-induced fluorescence at approximately 1 kHz. For each droplet the ratio of emitted fluorescence intensities at 580 nm and 630 nm is calculated in real time.

3. 11 mtDNA sequencing and copy number quantification

In collaboration with Dr. Leonardo Caporali (IRCCS Istituto delle Scienze Neurologiche, Bologna, Italy) we performed the mtDNA sequencing and copy number quantification. Sequence analysis of the entire mtDNA molecule was performed by Next Generation Sequencing (NGS) methods. Briefly, two long PCR amplicons (9.1 kb and 11.2 kb) were amplified using Q5 High-Fidelity DNA Polymerase (New England Biolabs, UK), purified by Agencourt AMPure XP (Beckman Coulter Life Sciences, Italy). The library was constructed by Nextera XT DNA Library Preparation Kit (Illumina, San Diego, CA) and sequenced on MiSeq System (Illumina, San Diego, CA), using the 600-cycle reagent kit. All the mutations are relative to the revised Cambridge Reference Sequence (rCRS, NC_012920). The complete mtDNA sequence of the samples have been deposited. All variants of interest were confirmed in all their available relatives by restriction fragment length polymorphism (RFLP) analysis (primers and conditions are available upon request). Mitochondrial DNA copy number was evaluated by qRT-PCR. Population frequencies of missense mutations and the mtDNA backgrounds on which they were observed were recovered from two public databases, Mitomap (http://www.mitomap.org) and HmtDB (http://www.hmtdb.uniba.it) [47,48]. Haplogroup affiliations of mitogenomes were assigned according to PhyloTree (www.phylotree.org).

3.12.1 Metabolomic samples preparation

GDS and GDR clones, derived from IGROV-1 were seeded at 1.000.000 cells in Petri dishes in a total volume of 10 mL in biological replicates (n = 3 for) for each clone. 48h or 72h after seeding, all clones were in exponential growth with quite same proliferation rate. After a period of incubation at 37° C, cells were washed two times with PBS and one wash with H2O milli Q. Then, we poured 10 mL

liquid nitrogen into the plates for some seconds and when it is evaporated we closed the plates and finally we stored all of them at −80 °C.

Extraction was done by adding 1mL of ice-cold MeOH H2O (85:15) to each plate and cells were scraped. Extracts were transferred to 1.5mL micro-centrifuge tubes and pelleted at 4 °C for 15min at 10000×g. Supernatants were stored at −80 °C. Twenty µL of each supernatant were used for untargeted metabolomics analysis.

3.12.2 Direct Flow Injection-TOF MS/MS

In collaboration with Dott. Roberta Pastorelli and Dott. Laura Brunelli, GDR and GDS cell clones were extracted and analyzed within seven days. The analysis was performed on an Agilent 1290 infinity Series coupled to an Agilent 6550 iFunnel Q-TOF mass spectrometer (Agilent, Santa Clara, CA) equipped with an electrospray source operated in negative and positive mode. The flow rate was 150 µL/min of mobile phase consisting of isopropanol/water (60:40, v/v) buffered with 5 mM ammonium at pH 9 for negative mode and methanol/water (60:40, v/v) with 0.1% formic acid at pH 3 for positive mode. Reference masses for internal calibration were used in continuous infusion during the analysis (m/z 121.050873, 922.009798 for positive and m/z 11.9856, 1033.9881 for negative ionization). Mass spectra were recorded from m/z 50 to 1100. Source temperature was set to 320 C with 15 L/min drying gas and a nebulizer pressure of 35 psig. Fragmentor, skimmer, and octopole voltages were set to 175, 65, and 750 V, respectively. MS/MS fragmentation pattern of the significantly features were collected and used to confirmed metabolite identity.

3.12.3 Data Processing and Metabolite identification

All steps of data processing and analysis were performed with Matlab (The Mathworks, Natick) using in-house developed pipeline. Briefly, in this procedure,

we applied a cutoff to filter peaks of less than 500 ion counts for negative and 1000 ion counts positive ionization ion counts to avoid detection of background features. Centroid m/z lists from different samples were merged to a single matrix by binning the accurate centroid masses within the tolerance given by the instrument resolution (about 20 ppm). The resulting matrix lists the intensity of each mass peak in each analyzed sample. Because mass axis calibration is applied online during acquisition, no m/z correction was applied during processing to correct for potential drifts. Singular metabolic species were identified by database searches (METLIN, http://metlin.scripps.edu; HMBD, http://www.hmdb.ca/; in positive and negative ionization.

3.13 Flow cytometry: Annexin-V Apoptosis Assay

To evaluate cytotoxic effects of Metformin on clones, we plated $2 \cdot 10^5$ cells per well in 6-wells tissue culture plates. The following day, the medium was changed and we treated cells. Cell viability was evaluated following 48 hours of Metformin treatment, using Annexin V/PI Staining Kit (Roche Applied Sciences; Penzberg, Germany). Cells were stained with 2 μl Annexin-V Fluos, 2 μl propidium iodide and 100 μl Hepes buffer, according to the manufacturer's instruction. Following an incubation of 15 minutes in the dark, staining was blocked with 200 μl Hepes buffer and results were expressed as cell viability, considering the percentage of Annexin V-/PI- cells at the experimental time point.

3.14 GeneChip Analysis

RNA quality and purity control were assessed with the Agilent Bioanalyzer 2100 (Agilent Technologies, Waldbronn, Germany) using "Eukaryote total RNA Assay".

To perform gene expression experiments, extremely high quality of total RNA was used (RIN≥9).

Only RNA samples that passed the quality controls were diluted to 100 ng in a total volume of 3 µl DEPC treated water to perform gene expression experiments. In vitro transcription, hybridization and biotin labelling were performed according to GeneChip 3'IVT Express kit protocol (Affymetrix, Santa Clara, CA). The Affymetrix GeneChip Scanner was used to measure all intensities of the signals of each probe set on the GeneChip and stores all signals in a .DAT file (Raw image). Integrated software converts all raw signals into numbers, which were stored in a .CEL file. All GEP profiles used in these experiments were assessed for their comparability and quality, using different quality controls: Scale Factor, number of present calls, internal probe calls, Poly-A controls and the ratio GAPDH/β-actin 3'/5'.

Bioinformatic analysis of gene expression microarray data was carried out in the R statistical environment using Bioconductor packages. Data were preprocessed using the RMA algorithm. Differential expression analysis was performed in the limma package, by linear model, moderating the t-statistics by empirical Bayes shrinkage. To correct for multiple testing, the Benjamini and Hochberg's method was applied, fixing the false discovery rate (FDR) cut-off at 0.01. Gene Set Enrichment Analysis (GSEA) was performed to evaluate the functional significance of curated sets of genes (*77*). Genes were ranked by moderated t-statistics and GSEA pre-ranked was run with default parameters, using gene set collections in the Molecular Signatures Database v6.2 (http://www.broadinstitute.org/gsea/msigdb/index.jsp). Specifically, we tested the significance of KEGG and Biocarta pathways, present in the "c2.cp.kegg" and "c2.cp.biocarta" collections.

GeneChip® 3' IVT PLUS Reagent Kit (Primeviews) to analyze the GDR and GDS clones.

3.15 Western Blot analysis

Cells were resuspended in lysis buffer (NP-40 1%, NaCl 150 mM, Tris HCl pH7.5 50 mM, EDTA 2mM, NaF, Na3VO4 and protease inhibitor cocktail) and lysates obtained were quantified using Quantum protein Assay (Euroclone). About 30 µg of proteins were denaturated and loaded in a midi polyacrylamide gel 4-12% (Life Tecnologies). Separated proteins were then transferred for 2 h at 400mA on a nitrocellulose membrane (GE Health Care, Glattbrugg, Switzerland). Membranes were saturated for 1 hour with TBS - 0,1% Tween - 5% - milk and then incubated over night with primary antibodies at 4°C, according to manufacturer's instructions.

In this work, we used the following primary antibodies:

- Mouse anti-α-TUBULIN, 1:4000 (Sigma Aldrich);
- Rabbit anti-MCT1, 1:1000 (EMD Millipore, AB3538P)
- Rabbit anti-MCT4, 1:300 (Santa Cruz, Biotechnology. Sc-50329);

Membranes were washed 2 times for 15 minutes (un-phosphorylated antigens) and incubated for 1 hour with horseradish-conjugated secondary antibodies (Amersham-Pharmacia; Little Chalfont, UK). Detection was obtained using Western Lightning plus ECL reagents (PerkinElmer), containing Luminol, which is oxidized by horseradish peroxidase, resulting in light emission at 425 nm. Signals emitted were acquired using ChemiDoc™ XRS system (Bio-Rad; Hercules, CA, USA).

3.16 Cell count

Trypan blue staining is a long-standing and widely used method to detect dead and dying cells in cytotoxicity assays and for routine assessment of cell viability

and proliferative assays. Only cells with intact membranes can effectively exclude the dye, so dead cells with compromised membranes become stained. Trypan blue staining is the method employed on the Countess® Automated Cell Counter, and this 0.4% trypan blue solution is the correct concentration for use on that instrument.

3.17 Sulforhodamine B assay

The sulforhodamine (SRB) assay was used for cell density determination, based on the measurement of cellular protein content. It measures drug-induced cytotoxicity and cell proliferation for large-scale drug-screening of compounds to adherent cells in a 96-well format. After an incubation period, cell monolayers are fixed with 10% (wt/vol) trichloroacetic acid and stained for 1.30h, after which the excess dye is removed by washing repeatedly with 1% (vol/vol) acetic acid. The protein-bound dye is dissolved in 10 mM Tris base solution for OD determination at 510 nm using a microplate reader.

3.18 Animals and treatments

Xenografts were generated by injecting subcutaneously (s.c) into both dorsolateral flanks with 0.3×10^6 to 0.5×10^6 different ovarian tumor cells mixed at 4°C with liquid Matrigel (Becton-Dickinson) into severe combined immunodeficient (SCID) mice (Charles River). To study the metabolic heterogeneity as a mechanism of resistance after anti-VEGF therapy we used Anti-human VEGF monoclonal antibody (mAb; A4.6.1, Bevacizumab) that was administered intraperitoneally (i.p.) at 100 µg/dose every 2 days, and mice were sacrificed 48 hours after the tenth treatment. Control mice received i.p. injections of PBS.

Tumor volume (mm3) was measured by a caliper and calculated according to the following formula: L × l2 × 0.5, where L is the longest diameter, l is the shortest diameter, and 0.5 is a constant to calculate the volume of an ellipsoid. Procedures involving animals and their care were performed according to institutional guidelines that comply with national and international laws and policies (EEC Council Directive 86/609, OJ L 358, 12 December 1987).

3.19 Immunohistochemistry analysis (IHC)

Five-micron-thick formalin-fixed, paraffin-embedded (FFPE) tumor samples were stained by IHC, using rabbit-MCT1 antibody the Monocarboxylic acid transporter 1 (ab85021, abcam, Cambridge, UK) according to the manufacturer's instructions. IHC was performed using a Leica Bond III Autostainer (Leica). The automate analyzer reduces the possibility to committed errors.
Immuno-reactivity was scored semi-quantitatively for both the intensity and the proportion of cells staining: intensity was given scores 0-3 (no staining = 0; light staining = 1; moderate staining = 2; strong staining = 3) and proportion was given scores 1-6 (0-4% = 1; 5-20% = 2; 21-40% = 3; 41-60% = 4; 61-80% = 5; 81-100% = 6). The two scores were multiplied to obtain the final score from 0 to 18.

3.20 Statistical analysis

Results were expressed as mean value ± SD. Statistical analysis of data was performed using Student's t-test or Mann-Whitney test. Differences were considered statistically significant when P ≤ 0.05.

4. Results

4.1 Authentication of ovarian cancer cell lines by STR analysis

Initially, we profiled and validated the ovarian cancer cell lines used in this study by Short Tandem Repeat (STR) analysis. The number of repeats in the *microsatellites* included in the panel can be highly variable and their length represents a unique genetic identifier of any given cell line.

In the table below (Table 4.1), I report results of the set of 16 STR loci analyzed.

	IGROV1	OC316	SKOV3	A2780	OAW42	A2774
D3S1358	14, 15	16, 17,18	14	14, 16	15, 16	16, 18
TH01	6, 9.3	6, 8	9, 9.3	6	6, 7	6, 8
D21S11	26, 30.2	30, 31	30, 31.2	28	26	30, 31
D18S51	15, 16	15	16, 17	16, 18	16, 21	14, 15
Penta E	13, 18	12, 13	5, 13	10, 13	12	13
D5S818	12	10, 12	11	11, 12	11, 12	10,12
D13S317	8, 9	8, 9	8, 11	12, 13	11	8, 9
D7S820	11	OL	13, 14	10	8	OL
D16S539	11	10, 11, 13	12	11, 13	12, 13	10,11, 12
CSF1PO	11, 14	10	11	10, 11	11	10
Penta D	8, 10	13, 14, 15	12, 13	8, 9	10	13,14, 15
vWA	17, 22	18, 19	17, 18	15, 16	15, 16	15, 19
D8S1179	14, 15	14, 15	14, 15	15, 17	13	14, 15
TPOX	8, 11	8	8, 11	8, 10	8, 11	8
FGA	20, 26	24	24, 25	19, 25	22, 25	24
AMELOGENIN	X	X	X	X	X	X

Table 4.1: results of STR loci analysis. The number of repeats mapping to each profiling locus detected in the various cell lines is reported.

Results show that the STR profiles of the various ovarian cancer cell lines match those reported in the literature (*78*).

4.2 Identification and characterization of clones with different survival under glucose starvation

By seeding cells at extremely low numbers (typically, 2, 1, 0.5 cells/well) through serial dilutions, we obtained 20-35 clones/cell line. Subsequently, clones were split and cultured in P96 wells either in the presence or in the absence of glucose (2 g/l). We evaluated their level of glucose addiction through daily observations at the optical microscope. We used the acronyms GDS and GDR to refer to Glucose Deprivation Sensitive or Glucose Deprivation Resistant clones, respectively (Figure 4.1).
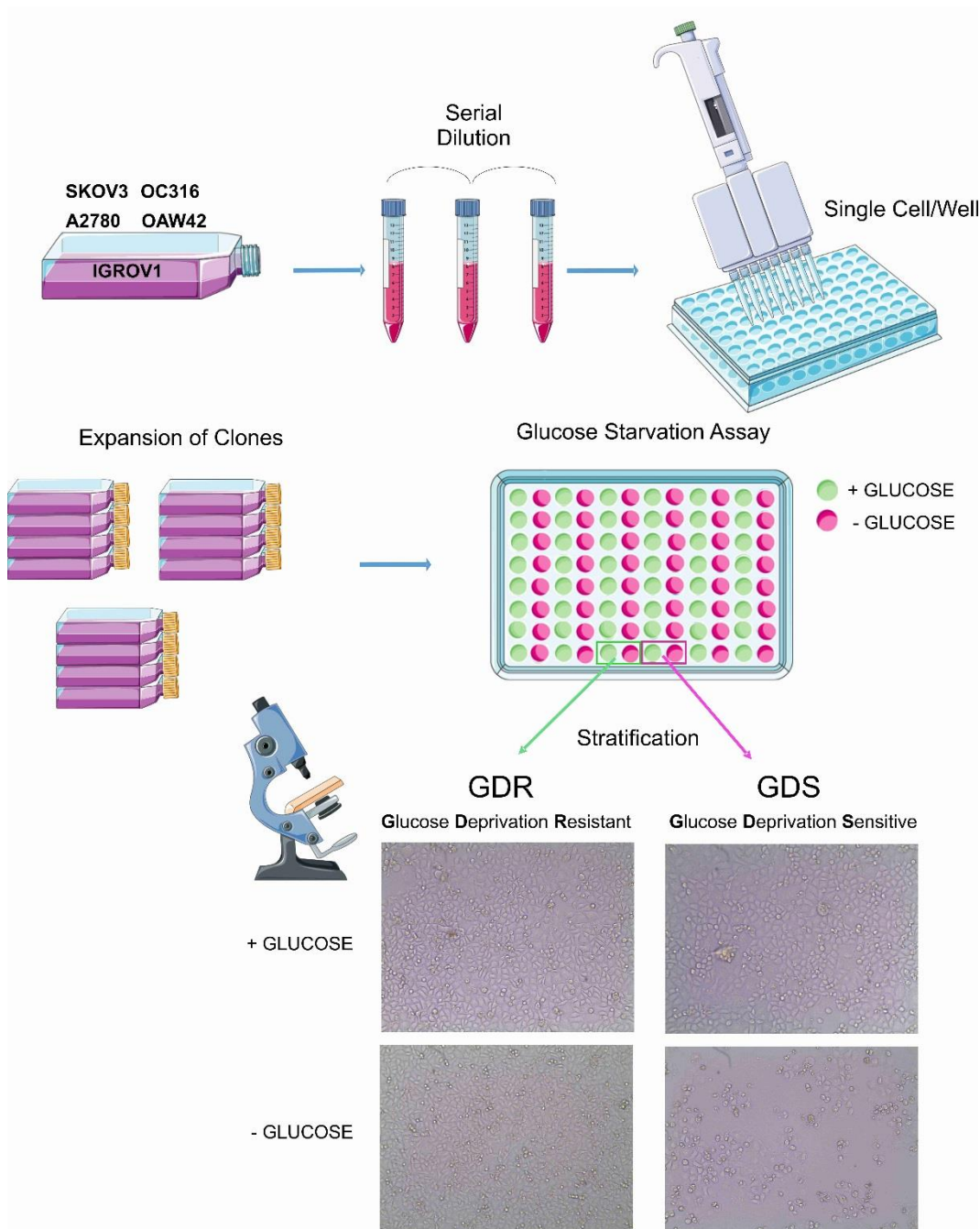
Figure 4.1: **Workflow of generation and characterization of GDR and GDS clones**. Isolation of single clones by limiting dilution analysis of IGROV-1, SKOV3, OC316, A2780, A2774 and OAW42 cells. Representative outcome of the glucose starvation assay after 72 h incubation.

We initially isolated several clones from different cancer cell lines, expanded them in tissue culture flasks and then performed the glucose starvation assay. Results suggest heterogeneous proportions of GDS and GDR clones in the various cell lines analyzed, ranging from 100% GDS clones in OC316 cells to 96% GDR clones in A2774 cells (Table 4.2).

	TOTAL CLONES	GDR	GDS	%GDR	% GDS	RATIO GDR/GDS
IGROV-1	20	11	9	55%	45%	1.2
OC316	35	0	35	0%	100%	0.0
SKOV3	21	10	11	48%	52%	0.9
A2780	15	22	9	87%	13%	2.4
OAW42	22	15	7	68%	32%	2.1
A2774	29	28	1	96%	4%	28.0

Table 4.2: **Proportions of GDR and GDS clones in ovarian cancer cell lines**. The table lists absolute numbers of clones obtained from the various cancer cell lines analyzed, the percentage of GDR and GDS clones and the GDR to GDS ratio.

We subsequently evaluated the glycolytic activity of these ovarian cancer cell lines through measurement of lactate production in the supernatants (Figure 4.2). In line with our previously published study (*49*), we confirmed that OC316 is an highly glycolytic cell line, whereas IGROV-1 are poorly glycolytic cells. The remaining ovarian cancer cell lines tested showed an intermediate glycolytic activity compared to IGROV-1 and OC316 cells, and we did not find any obvious correlation between amount of lactate production and proportions of GDS/GDR clones.
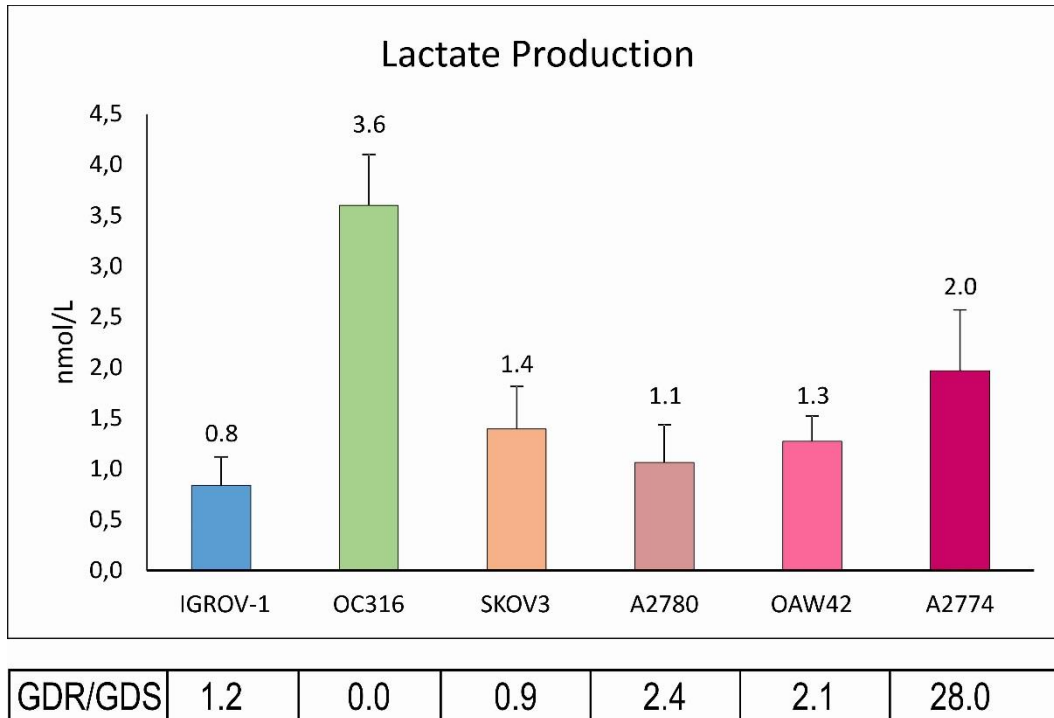
Figure 4.2: evaluation of glycolytic activity. Lactate concentrations in the supernatants of ovarian cancer cell lines collected 72 h after plating (2.5×10^5 cells in a P6 well).

4.3 Molecular and metabolic profile under standard culture conditions

4.3.1 The investigation of Glycolytic pathway

Following these preliminary observations, we performed in depth characterization of GDR and GDS clones established from IGROV-1 cells.

4.3.1.1 Analysis of transcripts associated with glycolysis in GDR and GDS clones

We evaluated expression of several canonical glycolysis-associated genes, including *GLUT1*, *GLUT3*, *HKII*, *GAPDH*, *LDHA*, *LDHB*, *MCT1* and *MCT4* (Figure 4.3). These genes codify for enzymes and transporters involved in different steps of glycolysis. Results of real time PCR experiments did not disclose significant

differences in the expression of any of these transcripts in GDR compared with GDS clones of IGROV-1 cells (Figure 4.3).
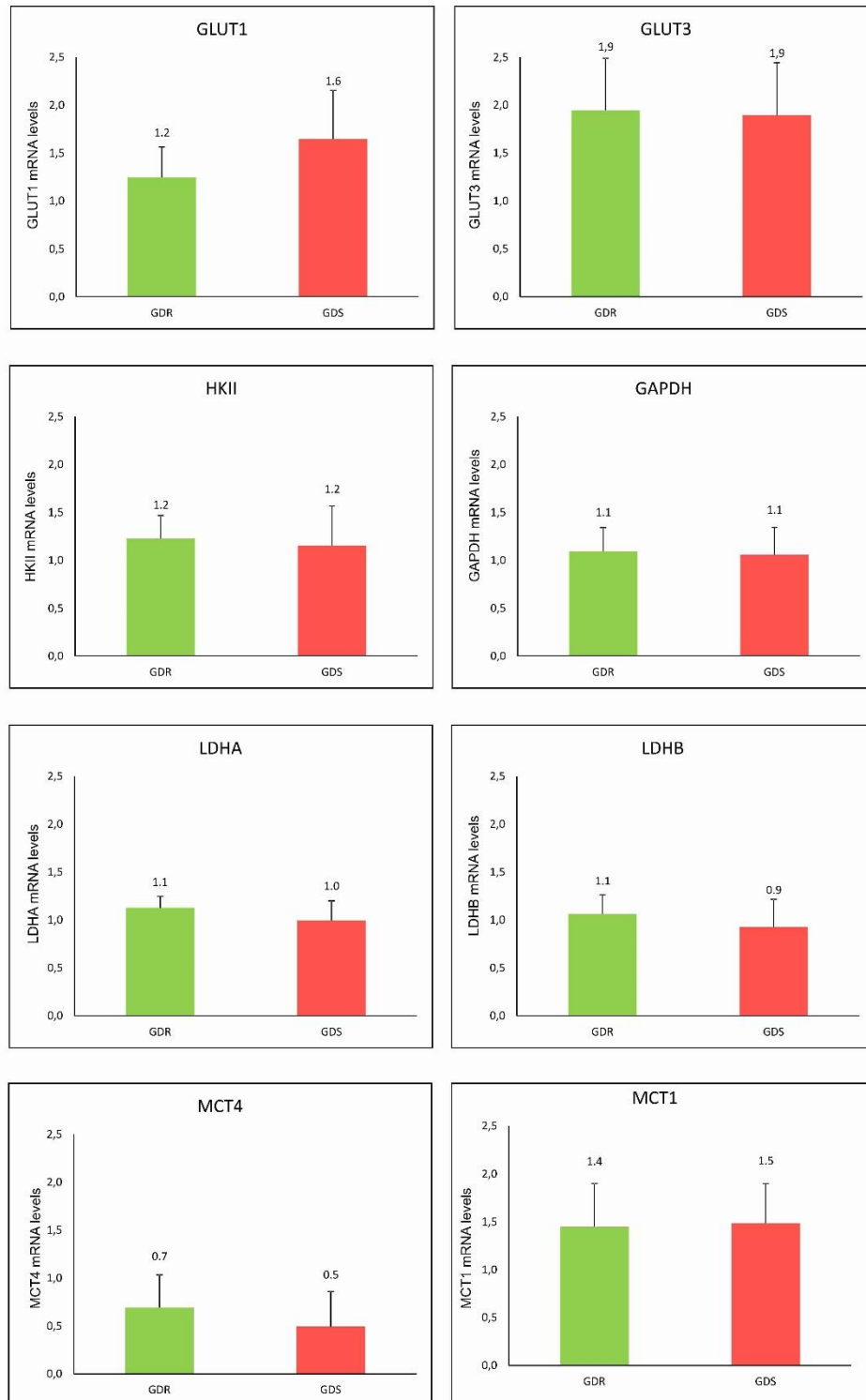
Figure 4.3: Measurement by Real Time PCR of glycolysis-associated transcripts in GDR and GDS clones established from IGROV-1 cells. Columns show mean values ± SD of 2 replicates of n=5 GDR (green columns) and n=5 GDS (red columns) clones. β2 microglobulin was used as housekeeping (p= ns).

4.3.1.2 Characterization of glycolytic metabolism by analysis of Glucose Consumption and Lactate Production

To start characterization of the metabolic features of GDR and GDS clones we measured glucose consumption and lactate production *in vitro*. To this end, clones were plated in P6 wells and after 72 h supernatants were collected and analyzed by colorimetric methods on an automated analyzer. Altogether, despite marked intra-group heterogeneity, similar glucose consumption and lactate production levels were measured in the supernatants of both GDR and GDS clones (Figure 4.4).
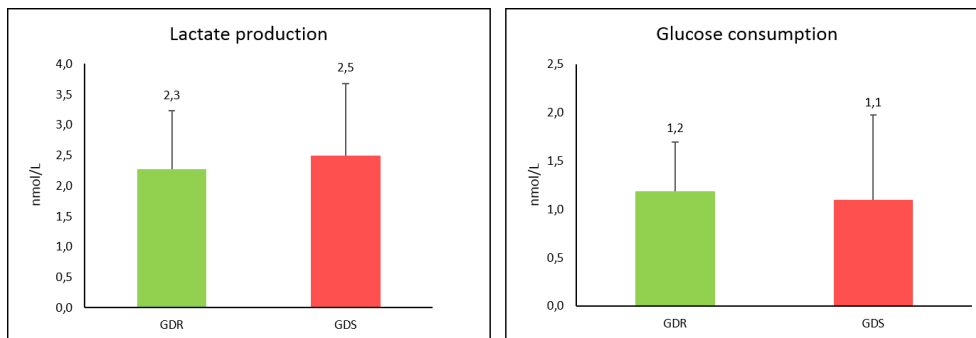
Figure 4.4: Measurements of lactate production and glucose consumption in GDR and GDS clones derived from IGROV-1 cells. Data are expressed as mean values (± SD) of n=15 GDR (green columns) and n=10 GDS (red columns) clones (p= ns). This analysis did not show significant differences between the two groups of clones.

4.3.1.3 Evaluation of Oxigen Consumption Rate (OCR) Extracellular Acidification Rate (ECAR) of GDR and GDS clones by Seahorse analysis

Seahorse analysis allows dynamic measure of the oxygen consumption rate (OCR) and extracellular acidification rate (ECAR). We applied this technique in collaboration with Dr. Ionica Masgras and Dr. Andrea Rasola (Department of Biomedical Sciences, University of Padova, Italy) to further investigate glycolysis and OXPHOS in GDR and GDS clones.

To this end, 2.5 x10^4 cells per well (n=5 replicates per sample) were plated in RPMI medium supplemented with 10% FBS. The following day, cells were placed in a running DMEM medium and pre-incubated for 30 minutes at 37°C in atmospheric CO2 before starting Seahorse measurements.

The cartridge of the instrument was loaded to dispense four different metabolic inhibitors at 20 min intervals including oligomycin, followed by carbonyl cyanide-4- (trifluoromethoxy)phenylhydrazone (FCCP), antimycin A and rotenone.

Results show a significant difference in the OCR values between clones GDR and GDS clones but not in ECAR values (Figure 4.5). Basal OCR value was significantly higher in GDR compared to GDS clones, suggesting increased OXPHOS activity in GDR clones. In contrast, ECAR was comparable between GDR and GDS clones, further supporting the lack of an obvious connection between glycolytic activity and the GDR/GDS phenotype.
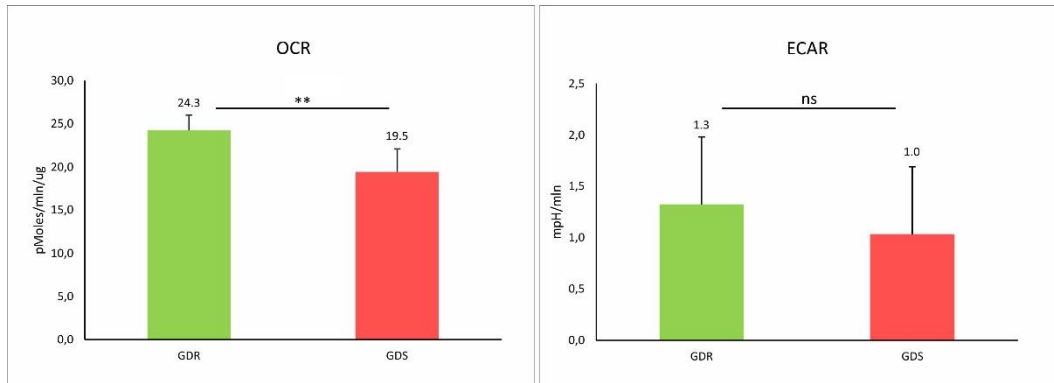
Figure 4.5: Seahorse analysis in GDR and GDS clones. This figure shows OCR (Oxigen Consuption Rate) and ECAR (Extracellular Acidification Rate) in GDR clones (green columns) and GDS clones (red columns). Columns show mean values ± SD of n=5 GDR or n=5 GDS indipendent samples, five technical replicates/sample (**p<0.01).

One of the four metabolic inhibitors used in Seahorse analysis was Oligomycin, a drug which inhibits ATP synthase and blocks respiration thus forcing the cells to use glycolysis. We observed that after Oligomycin treatment, the ECAR increased – as expected – both in GDR and GDS clones but GDR clones showed enhanced maximal glycolytic capacity compared to GDS clones.
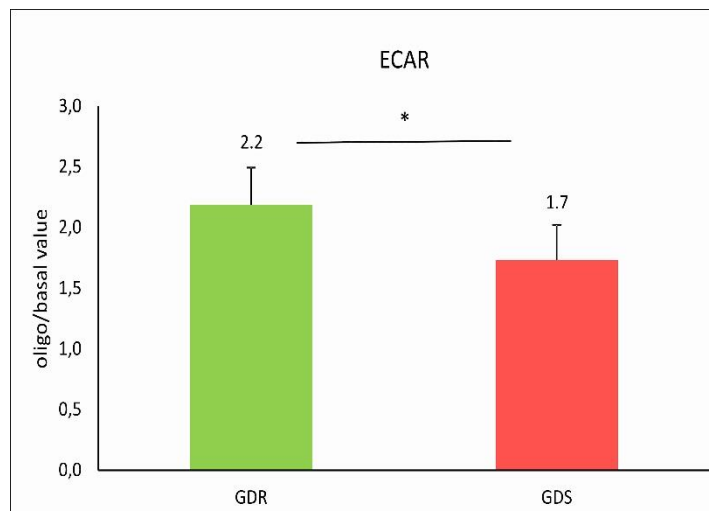
Figure 4.6: Extracellular Acidification Rate after Oligomycin. Data shown the normalization calculated by dividing the ECAR values after Oligomycin by ECAR basal values ± SD of 6 GDR and 5 GDS clones. GDR clones show increased maximal glycolytic activity compared with GDS clones (*p< 0.05).

In response to the mitochondrial uncoupling agent FCCP, GDS clones induced OCR lesser than GDR clones, indicating they have reduced spare respiratory capacities (Figure 4.7).
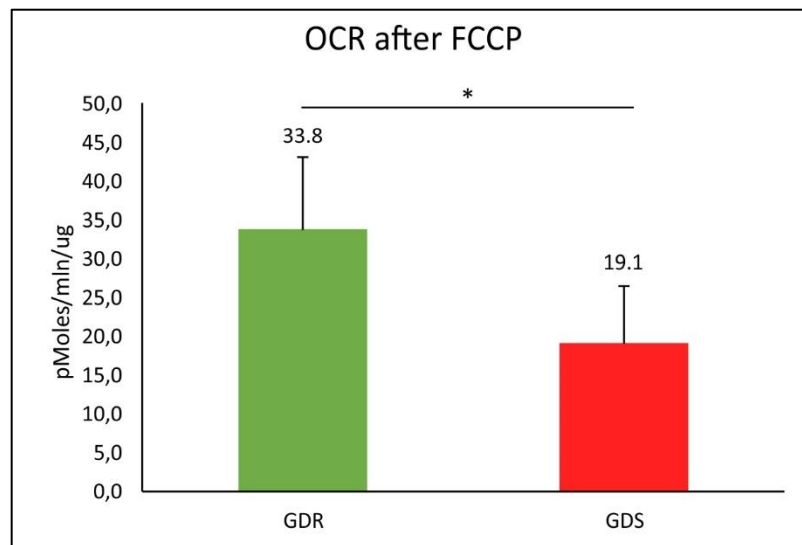
Figure 4.7: Oxygen Consumption Rate after FCCP. Data shown the OCR values after FCCP ± SD of 6 GDR and 5 GDS clones. GDR clones show increased Oxygen Consumption Rate compared with GDS clones (*$p < 0.05$).

4.3.1.4 Analysis of Single-Cell Metabolism in Droplet-Based Microfluidics

At the same time, we tried a different a methodology to discriminate GDR from GDS clones. In collaboration with Dr. Giulia Brisotto and Dr. Fabio Del Ben (Centro di Riferimento Oncologico, Aviano (PN), Italy), we performed a single-cell assay to detect lactate production. This technique is used to measure secretion of acid from individual living tumor cells compartmentalized in microfluidically prepared, monodisperse, picoliter (pL) droplets (*79*).

Analysis was performed both in GDR (12.19 and 10.4) and GDS (10.26 and 10.17) clones. Under standard culture conditions, GDR clones showed higher levels of acidification compared to GDS clones (Figure 4.8). These results were consistent with findings of Seahorse analysis (Figure 4.9). After Oligomycin treatment, we observed that GDR clones show more acidification compared to GDS clones. This phenomenon could be hypothetically explained by assuming that GDR cells

ground their metabolism on OXPHOS activity. When OXPHOS is inhibited (such as following Oligomycin treatment), cell metabolism is forced to switch to glycolysis. Conversely, GDS cell metabolism appears not to rely much on OXPHOS. Thus, OXPHOS blockade has relatively less impact on lactate production and acidification by GDS clones.
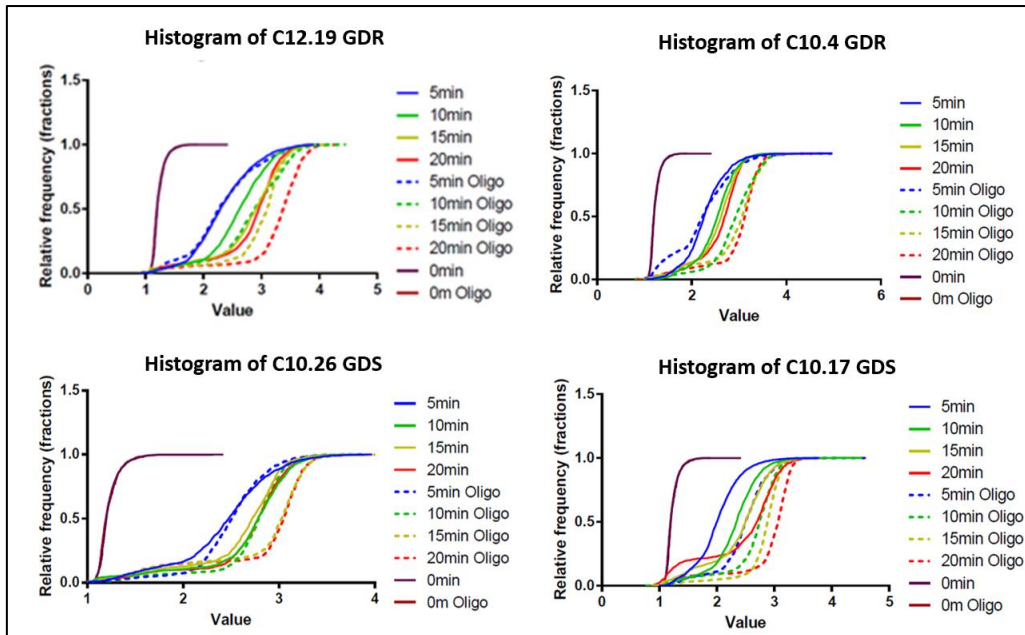
Figure 4.8: Analysis of single-cell metabolism of GDR and GDS clones (C12.19 and C10.4 GDR, C10.26 and C10.17 GDS). Value in X corresponds to the ratio 580/630 nm of SNARF-5F fluorescent signal that correlate with pH acidification. In this experiment, we tested in 4 time points (5, 10, 15 and 20 min represented with different colors) effects of Oligomycin on extracellular acidification. In the figure we can see that C12.19 GDR and C10.4 GDR have a high value of 580/630 ratio that correspond a high extracellular acidification compared to C10.26 GDS and C10.17 GDS.
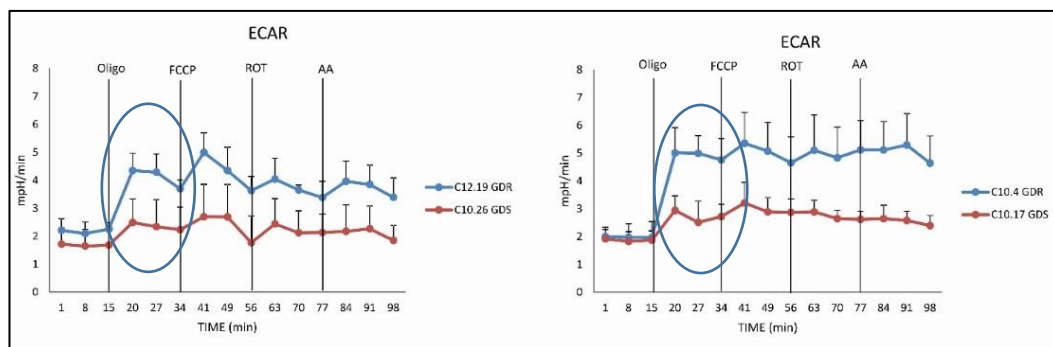
Figure 4.9: **ECAR values of two GDR and two GDS clones.** In light blue are represented the ECAR values of two GDR clones (C12.19, C10.4) and in red the ECAR values of two GDS clones (C10.26, C10.17). Subsequent additions of the ATP synthase inhibitor oligomycin, of the uncoupler FCCP, of the ETC complex I inhibitor rotenone, and of the respiratory complex III inhibitor antymicin A were carried out. Data are mean ± SD values of five replicates normalized to protein content.

4.3.2 The investigation of mitochondrial pathways

Previous findings suggest a difference in mitochondria activity in GDR and GDS clones. We investigated this possibility by a number of experimental approaches, as detailed below.

4.3.2.1 Metabolomics analysis of GDR and GDS clones

To obtain an overview of metabolic pathways dis-regulated in GDR compared with GDS clones, in collaboration with Dr. Laura Brunelli and Dr. Roberta Pastorelli (IRCCS-Istituto di Ricerche Farmacologiche Mario Negri, Milano, Italy) we performed untargeted metabolomics analysis of five GDR and five GDS clones. Metabolites were extracted with MeOH/H_2O (85:15) and samples were analyzed using HPLC-QTOF (high pressure liquid chromatography-QTOF) both in positive and negative ionization mode. Negative ionization highlighted mainly polar molecules and amino acids. Whereas, positive ionization discriminates mainly amino acids, acyl carnitine and lipids. Lipids were not considered in

untargeted data elaboration because there were not lipid standards. Differences among samples were investigated using multivariate statistical analysis (PCA/OPLS-DA) or univariate (Wilcoxon-Mann-Whitney, Tukey-Kramer $p<0.05$). Results showed 20 metabolites differentially expressed in GDR vs GDS clones (Figure 4.10A). Notably, GDR samples significant expressed more adenosine triphosphate (ATP) and oxidized glutathione compare to GDS clones.

A

Metabolites	Fold change GDRvsGDS
Histidine	1.50
Creatine	2.03
Arginine	1.69
3-Dehydroxycarnitine	1.08
Nutriacholic acid	-1.76
Lactic acid	-1.23
Succinic acid	-4.95
Taurine	1.29
Aspartic acid	1.70
Glutamine	-1.37
Glutamic acid	1.20
Glycerol 3-phosphate	-1.54
D-Glucose	-1.48
Citric acid	1.44
Palmitic acid	-1.92
Stearic acid	-1.87
Glutathione	1.10
Adenosine triphosphate	4.82
Uridine diphosphate-N-acetylglucosamine	2.17
Oxidized glutathione	3.46

B

Figure 4.10: A) bold metabolites identified using MS/MS fragmentation patterns and B) metabolic enrichment analysis. In table A, 20 metabolites differentially expressed in GDR vs GDS clones are listed. In Figure B, results of metabolic enrichment analysis (MetaboAnalyst) show the different pathways significant enriched.

The 20 significant metabolites were submitted to metabolic enrichment analysis (MetaboAnalyst) (Figure 4.10B). In red circles were reported 7 significant enrichment pathways with both $p<0.05$ and FDR<0.05. Pink circles represented 6 significant enrichment pathways with only $p<0.05$ and the orange circles highlight not significant altered pathway, but showed pathways strictly connected with at least one significant altered pathway. The majority of deregulated pathways were connected with mitochondrial functions. These pathways include citric acid and urea cycles pathways, arginine, proline and

glutamate metabolism. This result could suggest altered mitochondria oxidative phosphorylation (OXPHOS) activity in GDR compared with GDS clones.

4.3.2.2 Inhibition of mitochondria respiratory chain complex I by Metformin

To further investigate whether OXPHOS differences might occur in GDR compared with GDS clones, we performed some experiments with Metformin, a weak respiratory chain complex I inhibitor which is approved in humans as anti-diabetic drug. We measured cell death after 48 h of treatment by the Annexin V/PI assay. GDR clones were significantly more sensitive compared to GDS clones to metformin but selectively under glucose starvation (Figure 4.11). This result suggests that increased mitochondria activity detected in GDR clones might render them more responsive to Metformin *in vitro.*
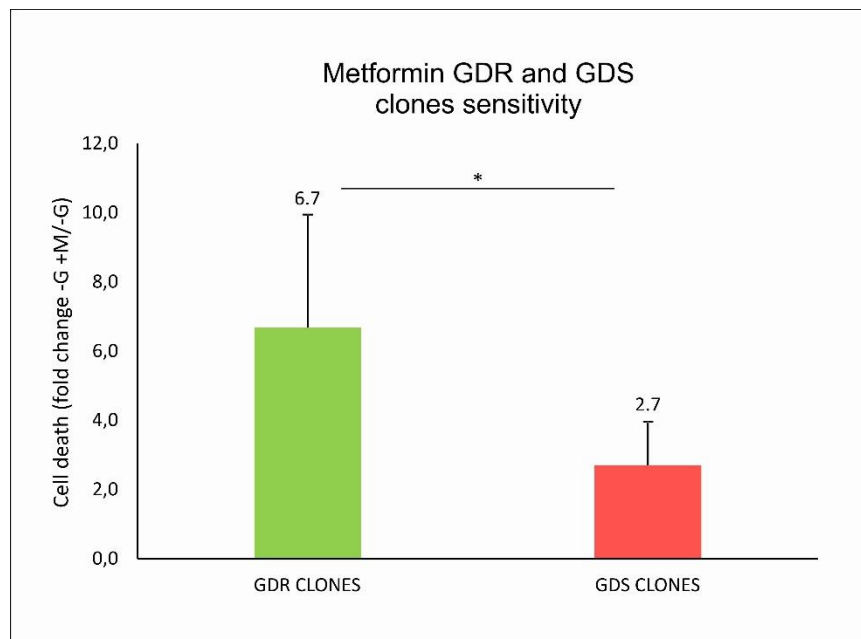
Figure 4.11: effects of Metformin under glucose starvation in GDR e GDS clones. Evaluation of Metformin effects in n=4 GDR and n=5 GDS clones by using the Annexin V/PI + cyfluorimetric assay. In the figure were reported the results normalized ± SD by dividing the values obtained under glucose starvation with or without metformin

treatment (1mM). GDR group was significantly sensitive compared to GDS clones to Metformin (*p<0.05).

4.3.2.3 Mitochondrial DNA analysis in GDR and GDS clones

To investigate whether these differences in OXPHOS and in particular the rather mild response of GDS clones to oligomycin and metformin could be due to mutations in mitochondria genes, we performed mitochondrial DNA analysis in collaboration with Dr. L. Caporali (Dipartimento di Scienze Biomediche e Neuromotorie, Bologna, Italy). We sequenced mitochondrial DNA from two GDR and two GDS clones but we did not find accumulation of deleterious mitochondrial DNA mutations in any samples (data not shown).

4.4 Transcriptional profiling of GDR and GDS clones under normal culture conditions

To investigate how these metabolic differences impact on the transcriptional profiling, we performed gene expression analysis of five GDR clones and five GDS clones derived from IGROV-1 cells under normal culture conditions. Differential expression analysis indicated that only 3 genes were significantly down-regulated, with FDR cut-off of 0.01 (data not shown). We thus performed a GSEA analysis to test whether a significant deregulation of canonical pathways could be observed in our dataset. GDR clones showed significant down regulation of several pathways, including RNA degradation, cell cycle progression, DNA replication and different DNA repair systems (FDR<0.05) compared to GDS clones. Notably, no up-regulated pathways were found, and we did not detect at the RNA level any modulations of pathways directly connected with mitochondrial respiration.

Glucose Deprivation Resistant (GDR) _vs_ Glucose Deprivation Sensitive (GDS)

clones under normal culture condition

NO UP-REGULATED PATHWAYS			
DOWN-REGULATED PATHWAY (29)	**N. of GENES**	**NES**	**FDR q-value**
KEGG_SPLICEOSOME	123	-2,92	0,000
KEGG_DNA_REPLICATION	36	-2,78	0,000
KEGG_PROTEASOME	43	-2,66	0,000
KEGG_AMINOACYL_TRNA_BIOSYNTHESIS	41	-2,53	0,000
BIOCARTA_FAS_PATHWAY	30	-2,48	0,000
KEGG_MISMATCH_REPAIR	23	-2,48	0,000
BIOCARTA_PROTEASOME_PATHWAY	28	-2,38	0,000
KEGG_CELL_CYCLE	124	-2,34	0,000
BIOCARTA_MCM_PATHWAY	18	-2,29	0,001
KEGG_BASE_EXCISION_REPAIR	33	-2,24	0,001
BIOCARTA_TNFR1_PATHWAY	29	-2,16	0,002
BIOCARTA_TID_PATHWAY	19	-2,12	0,003
KEGG_PATHOGENIC_ESCHERICHIA_COLI_INFECTION	56	-2,09	0,004
BIOCARTA_CDC42RAC_PATHWAY	16	-2,08	0,004
KEGG_RNA_DEGRADATION	55	-2,02	0,007
KEGG_PYRIMIDINE_METABOLISM	94	-1,97	0,009
BIOCARTA_HIVNEF_PATHWAY	58	-1,95	0,010
KEGG_NUCLEOTIDE_EXCISION_REPAIR	44	-1,93	0,012
KEGG_OOCYTE_MEIOSIS	110	-1,86	0,020
BIOCARTA_ATRBRCA_PATHWAY	20	-1,83	0,026
BIOCARTA_ARF_PATHWAY	17	-1,83	0,026
BIOCARTA_NFKB_PATHWAY	23	-1,81	0,029
BIOCARTA_CASPASE_PATHWAY	23	-1,80	0,029
KEGG_ONE_CARBON_POOL_BY_FOLATE	17	-1,79	0,029
BIOCARTA_ACTINY_PATHWAY	20	-1,79	0,029
BIOCARTA_RACCYCD_PATHWAY	26	-1,79	0,028
KEGG_PURINE_METABOLISM	150	-1,77	0,031
BIOCARTA_VEGF_PATHWAY	29	-1,72	0,045
KEGG_RNA_POLYMERASE	28	-1,70	0,049

Table 4.3: Gene Set Enrichment Analysis of five GDR clones _vs_ five GDS clones. The GSEA highlighted 29 pathways down-regulated in GDR vs GDS clones under standard culture conditions. No pathway was found to be up-regulated.

4.5 Molecular and metabolic features of GDR and GDS clones under glucose starvation

As phenotypic differences between GDR and GDS clones at optical microscopy are visible exclusively under glucose starvation, we reasoned that this experimental setting could be particularly informative about further molecular and metabolic differences involving these clones. To investigate this, we cultured

GDR and GDS clones under glucose starvation and then collected the samples for downstream analysis. We chose 48 h as time point for these analysis because at this time point glucose deprivation had cytostatic but not cytotoxic effects.

4.5.1. Analysis of glycolysis-associated transcripts and proteins by Real Time PCR and Western Blot assay

First, we measured expression of several glycolytic genes (*GLUT3, HKII, GAPDH, LDHA*, *LDHB, MCT1* and *MCT4*) by Real Time PCR. We did not find any substantial difference in the expression of *GLUT3, HKII, GAPDH, LDHA, LDHB* and *MCT4* transcripts in GDR compared to GDS clones under glucose starvation. On the other hand, we observed a significant difference in *MCT1* transcript expression under glucose starvation (Figure 4.12). MCT1 controls the reversible exchange of pyruvate and lactate between the cytosol and extracellular space. This carrier is also involved in pyruvate import in the mitochondria.

We evaluated MCT1 protein expression under the same conditions, with and without glucose (Figure 4.13). We noticed that in 4 out of 6 GDR clones analyzed there was up-regulation of MCT1 protein under glucose starvation (Figure 4.13). Altogether, results showed significant up-regulation of this protein in GDR clones (Figure 4.14). In contrast, expression of MCT1 protein did not substantially change in the absence of glucose in GDS clones (Figure 4.14).

Moreover, MCT4 was expressed at low levels in IGROV-1 clones and we did not observe obvious differences in MCT4 protein expression under glucose starvation (Figure 4.13).

In conclusion, GDR clones seem to react to glucose starvation through up-regulation of MCT1 transcript and protein. We speculate that cells import pyruvate from the extracellular microenvironment and use this metabolite for cell survival under glucose starvation.
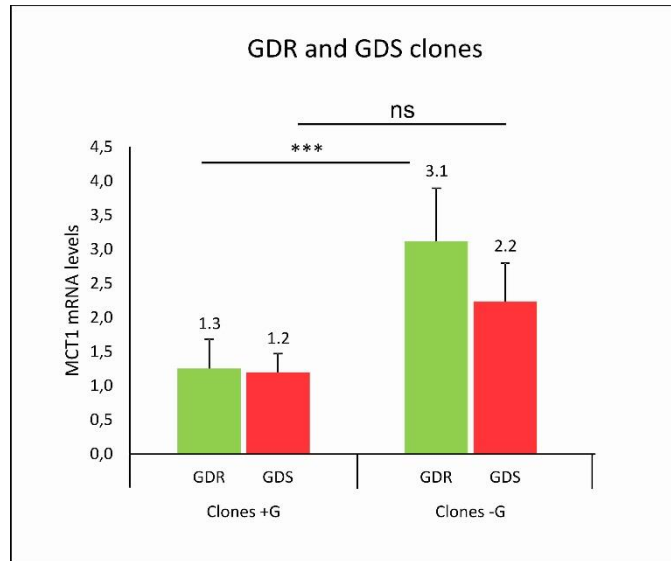
Figure 4.12: evaluation by Real Time PCR of MCT1 mRNA levels in GDR and GDS clones under normal and glucose starvation conditions. MCT1 mRNA levels in n=5 GDR and n=5 GDS clones cultured in presence or absence of glucose (2g/L). Columns show mean values ± SD of two replicates. β2 micro globulin was used as housekeeping (*** p<0.001).
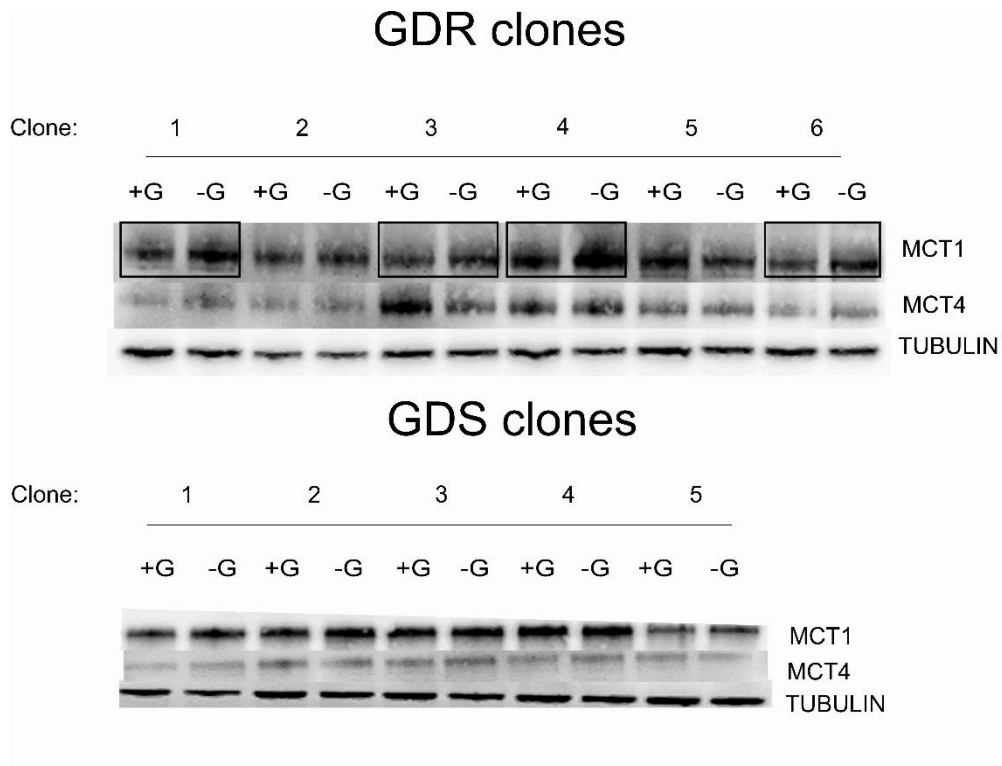
Figure 4.13: MCT1 and MCT4 Western blot analysis in GDR and GDS clones. MCT1 and MCT4 protein levels in n=6 GDR and n=5 GDS clones cultured in presence (+G) or absence of glucose (-G) (2g/L). α-tubulin was used as loading control. Western blot analysis showed a up-regulation of MCT1 protein In four of six GDR clones. MCT4 did not show differences under glucose starvation condition compared to normal condition.
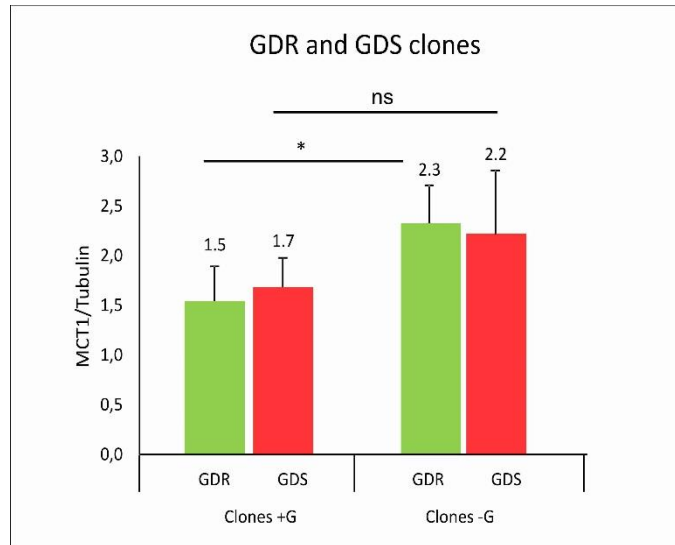
Figure 4.14: MCT1 protein quantification. The graph shows mean expression normalization ± SD of MCT1 protein divided by α Tubulin as load control, in n=6 GDR (green columns) and n=5 GDS (red columns) clones cultured for 48 h under normal conditions or glucose starvation. MCT1 protein expression showed a significant difference in GDR clones under glucose starvation compared to standard conditions (*p< 0.05).

4.5.2 Role of pyruvate in GDR and GDS clones

Pyruvate is produced during glycolysis and it can also be derived from additional sources in the cytoplasm. Pyruvate is ultimately transported into mitochondria where it is the master fuel input undergirding citric acid cycle carbon flux. Accordingly, pyruvate is essential for mitochondrial ATP generation and for driving several major biosynthetic pathways intersecting the citric acid cycle (*80*). This metabolite is transported by MCTs intramembrane carriers (*81*).

As GDR clones up-regulate MCT1 expression under glucose starvation, we speculated that pyruvate could be used by these cells to maintain cell viability under glucose starvation. To test this hypothesis, we evaluated effects of pyruvate deprivation on GDR clones viability. We plated some GDR clones in P6 wells and cultured these clones under different culture conditions (with glucose,

without glucose, without glucose and pyruvate). As shown in Figure 4.15, combined deprivation of glucose and pyruvate caused massive cell death in GDR clones. We did not perform this experiment with GDS clones because these clones are by definition sensitive to glucose deprivation.

To confirm these results with another methodology we performed a cell density assay. Results of SRB assay showed substantial vulnerability of GDR clones to double starvation, compared to glucose starvation (Figure 4.16).
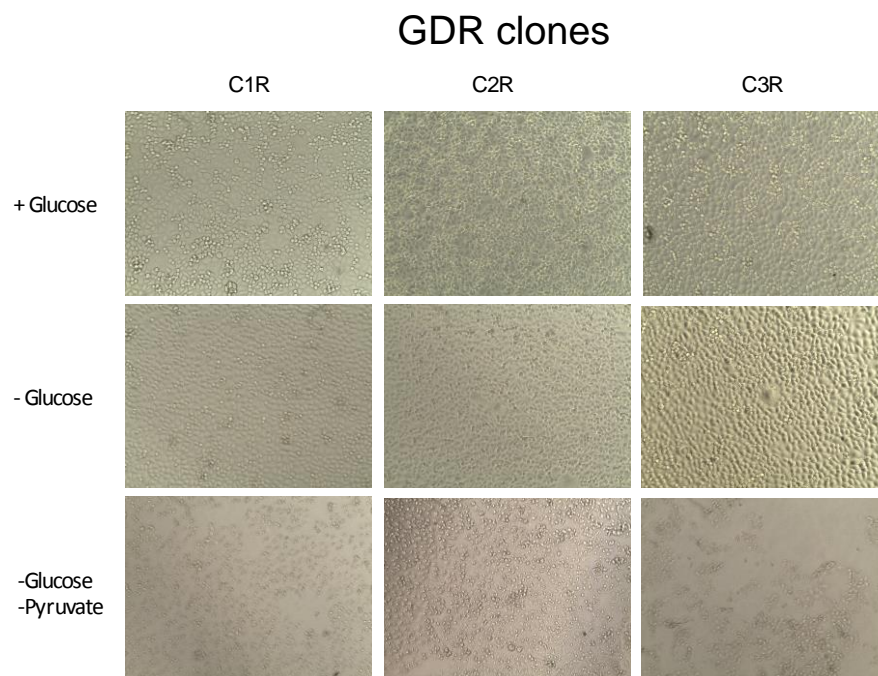
GDR clones

Figure 4.15: **Effects of pyruvate and glucose starvation on GDR clones.** Cell viability was evaluated by optical microscopy. GDR clones became sensitive to combined starvation (-Glucose -Pyruvate).
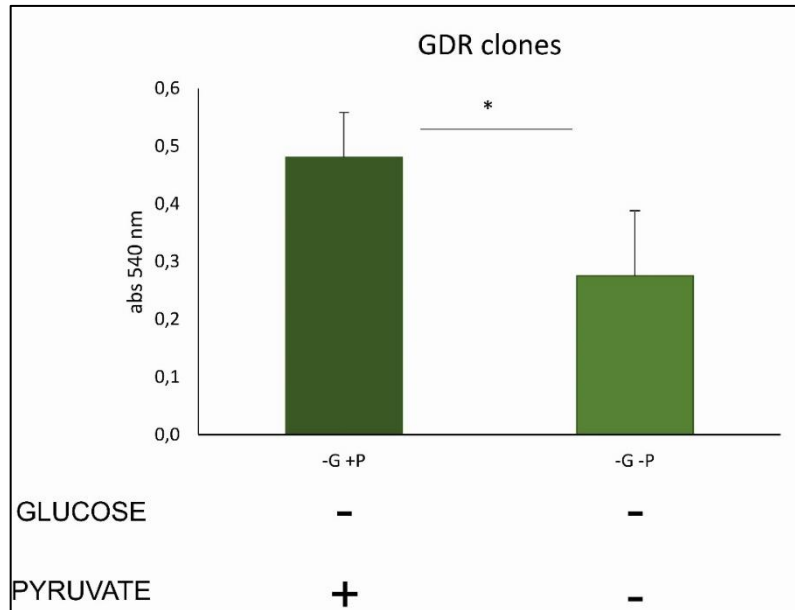
Figure 4.16: SRB assay under pyruvate and glucose starvation. The graph represents the mean values ± SD of 6 GDR clones under glucose starvation (-G +P) or glucose/pyruvate starvation (-G -P). Cell viability was measured at 540 nm. Combined deprivation caused significant effects in GDR clones compared to glucose starvation (*p<0.05).

4.5.3 Inhibition of MCTs transporters by Lonidamine

Recently, Lonidamine (LND) has been reported as potential MCTs inhibitor. LND inhibits import and export of pyruvate and lactate from the cells and inhibits pyruvate import in the mitochondria (*82*).

We tested this compound in GDR and GDS groups under different conditions of starvation induced stress. We used automated cell counter to evaluate effects of Lonidamine in the presence or absence of glucose and compared results obtained in the two types of clones. We used Lonidamine at a concentration (253 µM) which corresponds to the IC50 calculated in IGROV-1 cells; we chose 48 h time point to minimize cell death under glucose starvation, as already reported above. We observed that LND had similar effects both in medium containing

glucose or without glucose, apparently without selectivity of GDR or GDS clones (Figure 4.17).

In this experiment, we also cultured cells under pyruvate starvation. We obtained comparable results between glucose starvation condition (–G) and pyruvate starvation condition (+G -P) in GDR and GDS clones (Figure 4.17). We did not obtain significant difference between the two groups. The double deprivation of glucose and pyruvate (–G -P) was comparable between the two groups of clones.

Our experiment suggested that LND had citotoxic effects both in the presence or absence of glucose in GDR and GDS clones. There was no apparent difference between the two groups of clones in the response to LND.
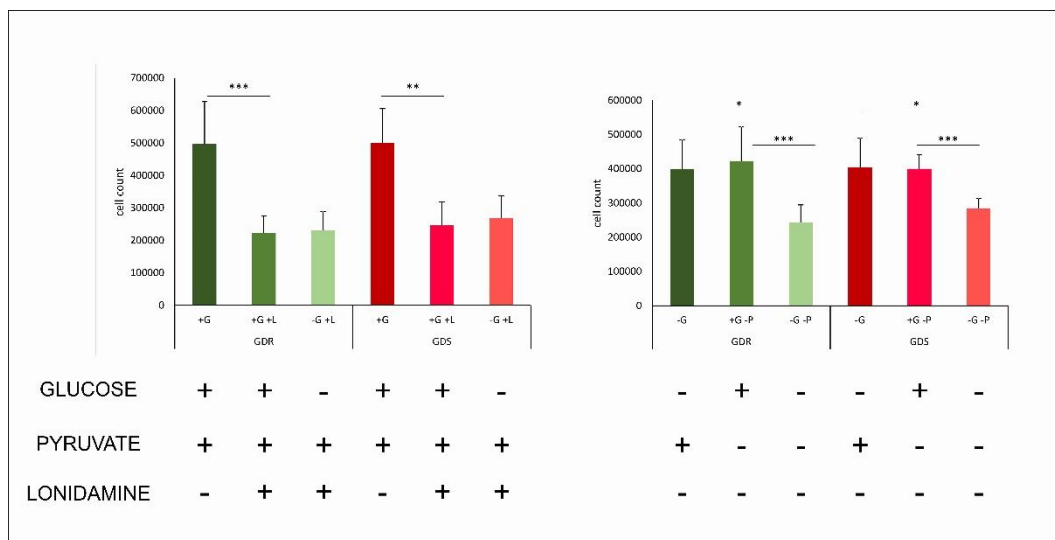
Figure 4.17: Glucose, Lonidamine and Pyruvate deprivation tested by cell count in n=5 GDR and n=5 GDS clones. Columns represent mean values of cell count of n=5 GDR and n=5 GDS clones ± SD. Lonidamine that we used at 253 µM, acted significantly with and without glucose in GDR and GDS clones (***$p<0.001$; **$p<0.01$). The double pyruvate and glucose deprivation caused a significant cytotoxic and cytostatic effect in GDR and GDS clones compared to pyruvate starvation (***$p<0.001$) and glucose starvation (*$p<0.05$). Notably, the similar effect of glucose compared to pyruvate starvation.

4.5.4 Transcriptional profiling of GDR and GDS clones under glucose starvation

To assess the impact of glucose starvation on the transcriptome, we performed gene expression analysis of five GDR and five GDS IGROV-1 clones cultivated for 48 h under glucose starvation. Differential expression analysis showed that only 9 genes were significantly modulated, 5 up- and 4 down-regulated, with FDR cut-off =0.01 (data not shown). Thus, we executed a GSEA analysis to elicit significantly deregulated canonical pathways. Analogously to the results in section 4.4 (obtained under normal culture condition), we did not find any up-regulated pathway in GDR vs GDS clones, whereas we found 29 down-regulated pathways involved in DNA replication, cell cycle progression and different DNA repair systems (Table 4.4). These pathways were largely overlapping with those we previously found by comparing transcriptional profiles of GDR and GDS clones cultivated under standard conditions, suggesting that key transcriptional differences between the two types of clones are not substantially perturbed by *in vitro* culture conditions.

GSEA analysis of GDR *vs* GDS IGROV1 clones

cultivated under glucosestarvation

NO UP-REGULATED PATHWAYS			
DOWN-REGULATED PATHWAY (29)	**N. of GENES**	**NES**	**FDR q-value**
KEGG_CELL_CYCLE	124	-2,94	0,000
KEGG_DNA_REPLICATION	36	-2,66	0,000
KEGG_MISMATCH_REPAIR	23	-2,55	0,000
KEGG_SPLICEOSOME	123	-2,46	0,000
BIOCARTA_G2_PATHWAY	24	-2,38	0,000
BIOCARTA_MCM_PATHWAY	18	-2,30	0,001
BIOCARTA_FAS_PATHWAY	30	-2,30	0,000
KEGG_NUCLEOTIDE_EXCISION_REPAIR	44	-2,27	0,001
KEGG_OOCYTE_MEIOSIS	110	-2,27	0,001
KEGG_BASE_EXCISION_REPAIR	33	-2,24	0,001
KEGG_PROTEASOME	43	-2,10	0,004
BIOCARTA_TEL_PATHWAY	18	-2,05	0,006
BIOCARTA_ATRBRCA_PATHWAY	20	-2,05	0,006
BIOCARTA_CHREBP2_PATHWAY	41	-2,04	0,006
KEGG_RNA_DEGRADATION	55	-1,99	0,009
KEGG_RIBOFLAVIN_METABOLISM	15	-1,93	0,012
BIOCARTA_GPCR_PATHWAY	34	-1,91	0,015
KEGG_AMINOACYL_TRNA_BIOSYNTHESIS	41	-1,90	0,017
BIOCARTA_ATM_PATHWAY	19	-1,82	0,031
BIOCARTA_PROTEASOME_PATHWAY	28	-1,81	0,032
BIOCARTA_VEGF_PATHWAY	29	-1,81	0,031
BIOCARTA_BCR_PATHWAY	34	-1,81	0,031
BIOCARTA_TNFR1_PATHWAY	29	-1,80	0,030
BIOCARTA_CALCINEURIN_PATHWAY	18	-1,80	0,029
BIOCARTA_HIF_PATHWAY	15	-1,80	0,029
BIOCARTA_AKAPCENTROSOME_PATHWAY	15	-1,79	0,030
KEGG_HOMOLOGOUS_RECOMBINATION	26	-1,75	0,039
BIOCARTA_HIVNEF_PATHWAY	58	-1,73	0,042
KEGG_PYRIMIDINE_METABOLISM	94	-1,72	0,044

Table 4.4: GSEA of n=5 GDR vs n=5 GDS clones under glucose starvation. GSEA highlighted 29 pathways down-regulated in GDR vs GDS clones under glucose starvation. No significantly up-regulated pathway was found.

We compared GSEA results obtained from clones (either GDR or GDS) grown under standard culture conditions or glucose starvation. As shown in Figure 4.18, we found 11 gene sets selectively down-regulated in GDR clones compared with GDS clones under glucose starvation.

DOWN-REGULATED PATHWAYS

DOWN-REGULATED PATHWAYS UNDER NORMAL CONDITION (11)

BIOCARTA_TID_PATHWAY
KEGG_PATHOGENIC_ESCHERICHIA_COLI_INFECTION
BIOCARTA_CDC42RAC_PATHWAY
BIOCARTA_ARF_PATHWAY
BIOCARTA_NFKB_PATHWAY
BIOCARTA_CASPASE_PATHWAY
KEGG_ONE_CARBON_POOL_BY_FOLATE
BIOCARTA_ACTINY_PATHWAY
BIOCARTA_RACCYCD_PATHWAY
KEGG_PURINE_METABOLISM
KEGG_RNA_POLYMERASE

DOWN-REGULATED PATHWAYS UNDER GLUCOSE STARVATION (11)

BIOCARTA_G2_PATHWAY
BIOCARTA_TEL_PATHWAY
BIOCARTA_CHREBP2_PATHWAY
KEGG_RIBOFLAVIN_METABOLISM
BIOCARTA_GPCR_PATHWAY
BIOCARTA_ATM_PATHWAY
BIOCARTA_BCR_PATHWAY
BIOCARTA_CALCINEURIN_PATHWAY
BIOCARTA_HIF_PATHWAY
BIOCARTA_AKAPCENTROSOME_PATHWAY
KEGG_HOMOLOGOUS_RECOMBINATION

DOWN-REGULATED PATHWAYS UNDER NORMAL CONDITION AND UNDER GLUCOSE STARVATION (18)

KEGG_CELL_CYCLE	KEGG_PROTEASOME
KEGG_DNA_REPLICATION	BIOCARTA_ATRBRCA_PATHWAY
KEGG_MISMATCH_REPAIR	KEGG_RNA_DEGRADATION
KEGG_SPLICEOSOME	KEGG_AMINOACYL_TRNA_BIOSYNTHESIS
BIOCARTA_MCM_PATHWAY	BIOCARTA_PROTEASOME_PATHWAY
BIOCARTA_FAS_PATHWAY	BIOCARTA_VEGF_PATHWAY
KEGG_NUCLEOTIDE_EXCISION_REPAIR	BIOCARTA_TNFR1_PATHWAY
KEGG_OOCYTE_MEIOSIS	BIOCARTA_HIVNEF_PATHWAY
KEGG_BASE_EXCISION_REPAIR	KEGG_PYRIMIDINE_METABOLISM

Figure 4.18: Venn diagram showing the intersection of down-regulated pathways in GDR vs. GDS clones under different culture conditions. The figure shows the list of pathways down-regulated in GDR vs GDS clones under normal conditions (blue arrow) or under glucose starvation (red arrow).

To highlight gene sets associated with glucose starvation in each clone type, we performed also the following comparisons: <u>GDR -G vs GDR +G</u> and <u>GDS -G vs GDS +G</u> (Figure 4.19).

Bioinformatic analysis revealed a massive change in differential expression (more than 10,000 genes) induced by the transition from standard culture condition to glucose deprivation, for both GDR and GDS clones (data not shown). In order to better interpret this amount of data, we thus performed gene set enrichment analysis.

GSEA results for GDR clones showed 5 up-regulated and 75 down-regulated pathways in the glucose starvation condition with respect to standard culture condition. We obtained similar results in GDS group: 6 pathways were up-regulated, and 65 pathways were down-regulated in GDS clones cultured under glucose starvation versus standard condition.

The comparison of significantly down-regulated gene sets between GDR and GDS clones was reported in Figure 4.19. Specifically, GDR clones displayed significant down-regulation of RNA and lysine degradation pathways not present in GDS. On the contrary, GDS clones grown under glucose starvation showed down regulation of mitochondrial gene sets, such as folate and TCA cycle, not detected in GDR clones.

DOWN-REGULATED PATHWAYS

GDR - G VS GDR +G

GDS - G VS GDS +G

57 pathways

18 pathways

8 pathways

DOWN-REGULATED PATHWAYS IN GDR CLONES UNDER GLUCOSE STARVATION (18)

BIOCARTA_GPCR_PATHWAY
BIOCARTA_FCER1_PATHWAY
BIOCARTA_TFF_PATHWAY
KEGG_REGULATION_OF_ACTIN_CYTOSKELETON
BIOCARTA_CCR3_PATHWAY
BIOCARTA_IL2RB_PATHWAY
BIOCARTA_UCALPAIN_PATHWAY
KEGG_NON_SMALL_CELL_LUNG_CANCER
BIOCARTA_AT1R_PATHWAY
KEGG_RNA_DEGRADATION
BIOCARTA_INTEGRIN_PATHWAY
BIOCARTA_ETS_PATHWAY
KEGG_LYSINE_DEGRADATION
KEGG_MELANOGENESIS
KEGG_GLIOMA
KEGG_LONG_TERM_POTENTIATION
BIOCARTA_MCALPAIN_PATHWAY
BIOCARTA_LONGEVITY_PATHWAY

DOWN-REGULATED PATHWAYS IN GDS CLONES UNDER GLUCOSE STARVATION (8)

KEGG_CITRATE_CYCLE_TCA_CYCLE
BIOCARTA_MITOCHONDRIA_PATHWAY
KEGG_FC_GAMMA_R_MEDIATED_PHAGOCYTOSIS
BIOCARTA_BARRESTIN_SRC_PATHWAY
BIOCARTA_DEATH_PATHWAY
KEGG_INSULIN_SIGNALING_PATHWAY
BIOCARTA_BIOPEPTIDES_PATHWAY
KEGG_ONE_CARBON_POOL_BY_FOLATE

DOWN-REGULATED PATHWAYS IN GDR AND GDS CLONES UNDER GLUCOSE STARVATION (57)

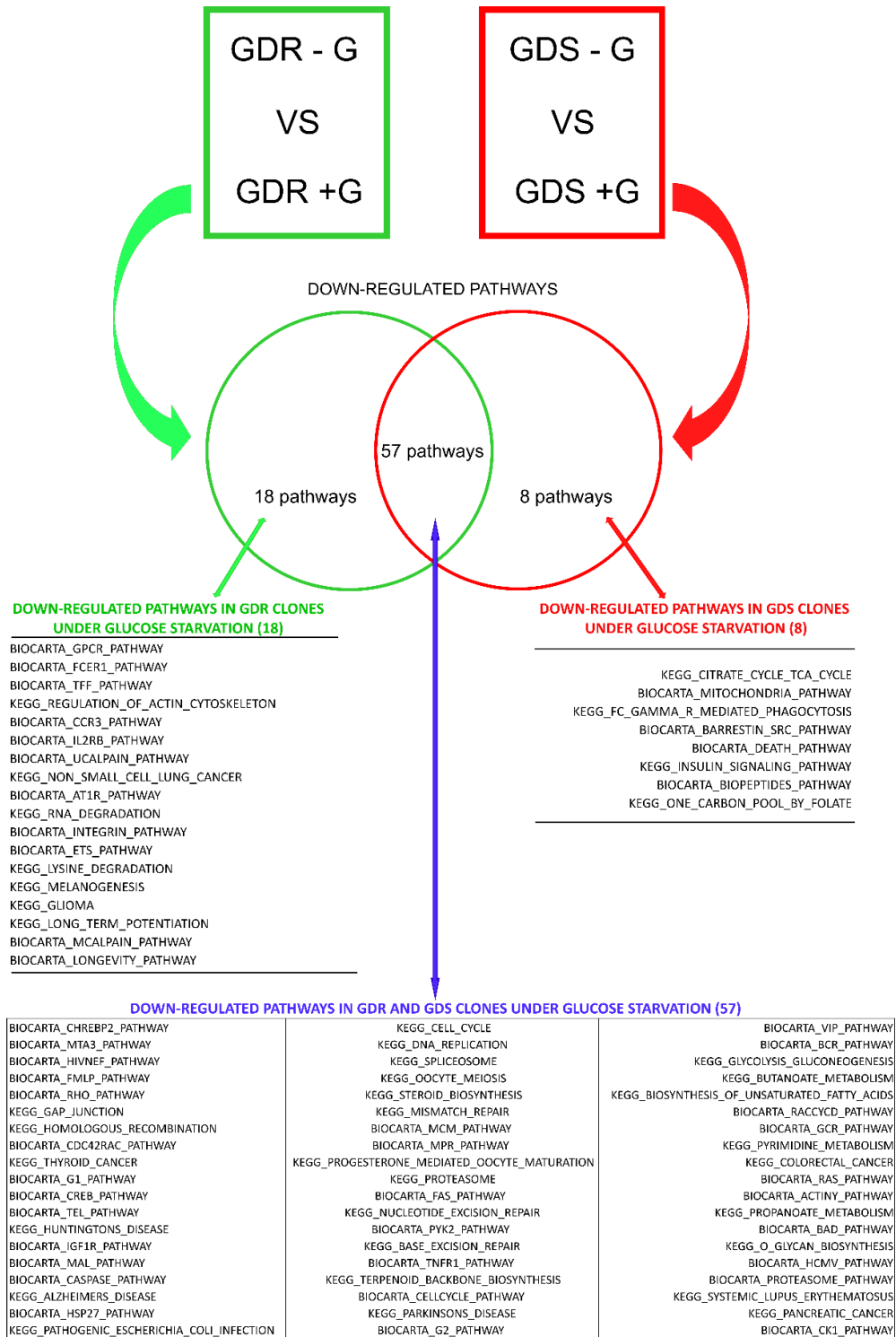|		
BIOCARTA_CHREBP2_PATHWAY	KEGG_CELL_CYCLE	BIOCARTA_VIP_PATHWAY
BIOCARTA_MTA3_PATHWAY	KEGG_DNA_REPLICATION	BIOCARTA_BCR_PATHWAY
BIOCARTA_HIVNEF_PATHWAY	KEGG_SPLICEOSOME	KEGG_GLYCOLYSIS_GLUCONEOGENESIS
BIOCARTA_FMLP_PATHWAY	KEGG_OOCYTE_MEIOSIS	KEGG_BUTANOATE_METABOLISM
BIOCARTA_RHO_PATHWAY	KEGG_STEROID_BIOSYNTHESIS	KEGG_BIOSYNTHESIS_OF_UNSATURATED_FATTY_ACIDS
KEGG_GAP_JUNCTION	KEGG_MISMATCH_REPAIR	BIOCARTA_RACCYCD_PATHWAY
KEGG_HOMOLOGOUS_RECOMBINATION	BIOCARTA_MCM_PATHWAY	BIOCARTA_GCR_PATHWAY
BIOCARTA_CDC42RAC_PATHWAY	BIOCARTA_MPR_PATHWAY	KEGG_PYRIMIDINE_METABOLISM
KEGG_THYROID_CANCER	KEGG_PROGESTERONE_MEDIATED_OOCYTE_MATURATION	KEGG_COLORECTAL_CANCER
BIOCARTA_G1_PATHWAY	KEGG_PROTEASOME	BIOCARTA_RAS_PATHWAY
BIOCARTA_CREB_PATHWAY	BIOCARTA_FAS_PATHWAY	BIOCARTA_ACTINY_PATHWAY
BIOCARTA_TEL_PATHWAY	KEGG_NUCLEOTIDE_EXCISION_REPAIR	KEGG_PROPANOATE_METABOLISM
KEGG_HUNTINGTONS_DISEASE	BIOCARTA_PYK2_PATHWAY	BIOCARTA_BAD_PATHWAY
BIOCARTA_IGF1R_PATHWAY	KEGG_BASE_EXCISION_REPAIR	KEGG_O_GLYCAN_BIOSYNTHESIS
BIOCARTA_MAL_PATHWAY	BIOCARTA_TNFR1_PATHWAY	BIOCARTA_HCMV_PATHWAY
BIOCARTA_CASPASE_PATHWAY	KEGG_TERPENOID_BACKBONE_BIOSYNTHESIS	BIOCARTA_PROTEASOME_PATHWAY
KEGG_ALZHEIMERS_DISEASE	BIOCARTA_CELLCYCLE_PATHWAY	KEGG_SYSTEMIC_LUPUS_ERYTHEMATOSUS
BIOCARTA_HSP27_PATHWAY	KEGG_PARKINSONS_DISEASE	KEGG_PANCREATIC_CANCER
KEGG_PATHOGENIC_ESCHERICHIA_COLI_INFECTION	BIOCARTA_G2_PATHWAY	BIOCARTA_CK1_PATHWAY

Figure 4.19: Venn diagram showing down-regulated pathways in GDR and GDS clones cultured under glucose starvation. Comparison of pathways down-regulated in GDR and GDS clones. We observed some pathways including mitochondria pathway, folate and TCA cycle selectively down-regulated in GDS clones when grown under glucose starvation.

4.6 Evaluation of proliferative activity of GDR and GDS clones

One of the most down-regulated pathway observed by transcriptome analysis in GDR clones was cell cycle progression. For this reason, we investigated proliferation of GDR and GDS clones growth *in vitro.* We plated in 7.500 cells/P96 well for each clone and after 16, 24, 48 and 72 h we performed SRB assay. We did not find any difference between GDR and GDS groups in terms of proliferation (Figure 4.20).
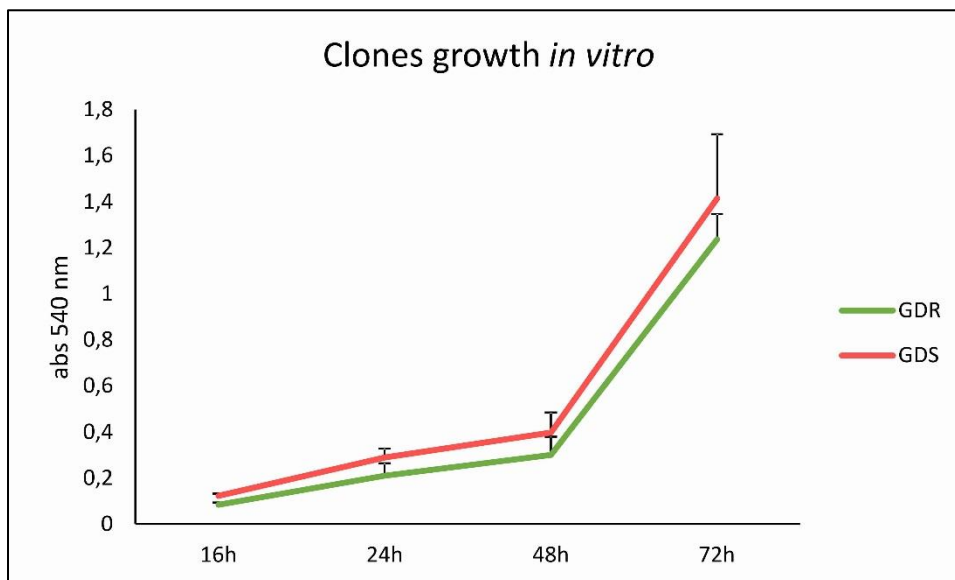

Figure 4.20: evaluation of clones proliferation *in vitro* by SRB assay. The figure shows mean values ± sd of n=4 GDR or n=4 GDS indipendent samples, 5 technical replicates/sample.

4.7 Analysis of tumorigenic potential of GDR and GDS clones

We investigated the tumorigenic capacity of GDR and GDS clones *in vivo*. To this end, 400.000 cells from GDR or from GDS clones (n=5/group) were injected subcutaneously in SCID mice. We measured tumor volumes of each one subcutaneous mass. Results showed that 2 out of 5 GDS clones grew clearly

faster than the others (Figure 4.21A). On average, however, we did not find a significant difference between the kinetics of tumor growth of GDR and GDS clones (Figure 4.21B).
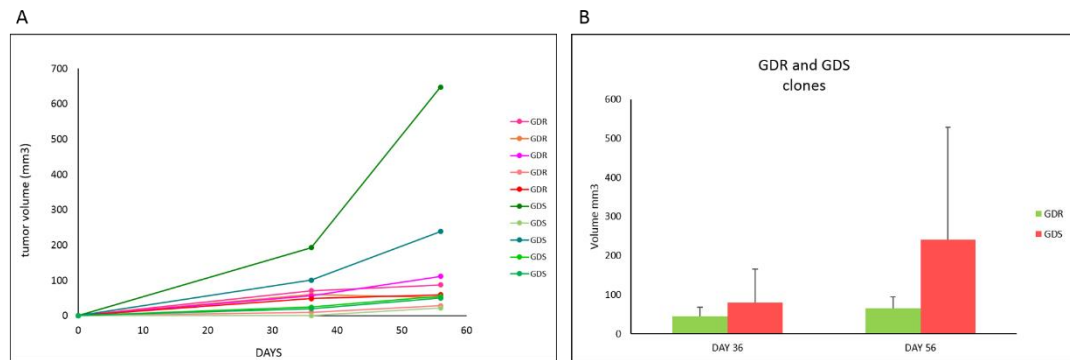

Figure 4.21: *in vivo* **growth of 5 GDR and 5 GDS clones.** A) Representation of tumors volume (mm^3) of GDR and GDS clones for 56 days. B) Means of tumors volume at 36 and 56 days ± SD. No significant difference was found between the two groups.

4.8 Characterization of GDR and GDS clones in *ex vivo* IGROV-1 cultures

Published studies from our and other laboratories, demonstrated that anti-VEGF therapy stably modulates the glycolytic phenotype of tumor cells in epithelial ovarian cancer (EOC) xenografts. This metabolic rewriting correlates with tumor aggressiveness and resistance to anti-angiogenic therapy (*49, 53, 83*). These studies, however, did not investigate the possible existence of metabolic heterogeneity in tumor samples treated with the antiangiogenic drug Bevacizumab.

To investigate this phenomenon, we set up an *in vivo* experiment with IGROV-1 cells. Following establishment of subcutaneous tumor xenografts, mice were treated with two or three weekly administrations of Bevacizumab (BEVA) for 4 weeks or PBS for control (CTRL) tumors. From these tumors treated or not, we

isolated the *ex vivo* cell cultures that we used to study the GDR and GDS clones percentage after anti-VEGF therapy.

We obtained n=136 total clones from n=5 CTRL tumor-derived samples and n=132 total clones from 5 BEVA tumor-derived cultures. In the case of CTRL clones groups, we found 51% and 49% GDR and GDS clones, respectively. This is a similar proportion to that obtained in IGROV-1 parental cells grown *in vitro*. In BEVA tumor-derived clones, we found 63% and 37% GDR and GDS clones, respectively. In this latter group, however, only the BEVA 5 culture contained an excess of GDS clones (27% GDR and 73% GDS clones) (Table 4.6). Due to the heterogeneity within each group, no statistically significant differences were found between CTRL and BEVA clones. For this reason, we aim to investigate the GDR and GDS clones percentage in other *ex vivo* culture samples. This preliminary result suggests that anti-VEGF therapy caused some perturbations in the balance of GDR/GDS clones in tumors with an enrichment of GDR clones in treated cultures.

	TOTAL CLONES	GDR	GDS	% GDR	% GDS
CONTROL 9	36	23	13	64	36
CONTROL 10	38	18	20	47	53
CONTROL 11	31	17	14	55	45
CONTROL 12	15	11	4	44	56
CONTROL 13	16	7	9	44	56
BEVACIZUMAB 1	30	27	3	90	10
BEVACIZUMAB 2	31	20	11	65	35
BEVACIZUMAB 5	33	9	24	27	72
BEVACIZUMAB 6	14	8	6	57	43
BEVACIZUMAB 7	24	18	6	75	25

Table 4.6: GDR and GDS clones ratio in 5 IGROV-1 *ex vivo* control cultures (CONTROL) and 5 *ex vivo* treated culture (BEVACIZUMAB). The table reports numbers and the percentage of clones isolated from 10 IGROV-1 *ex vivo* culture.

4.8.1 The evaluation of MCT1 protein in IGROV-1 tumor and ex vivo cultures

Previously, we observed that GDR clones had increased expression of MCT1 transcript and protein under glucose starvation. Thus, we speculated that

Bevacizumab-treated tumors, which are often enriched for GDR clones, could express more MCT1 protein compared to CTRL tumors.

Immuno-histochemical analysis of 6 treated tumors (BEVA) and 8 control tumors (CTRL) samples obtained at sacrifice, showed slightly increased MCT1 expression levels both in CTRL and BEVA groups (SCORE CTRL=9,6 ; SCORE BEVA=11,6. p=ns) (Figure 4.22). Notably, MCT1 staining in BEVA tumors seemed to be more defined and intense in cell membrane compared to CTRL tumors (Figure 4.22).
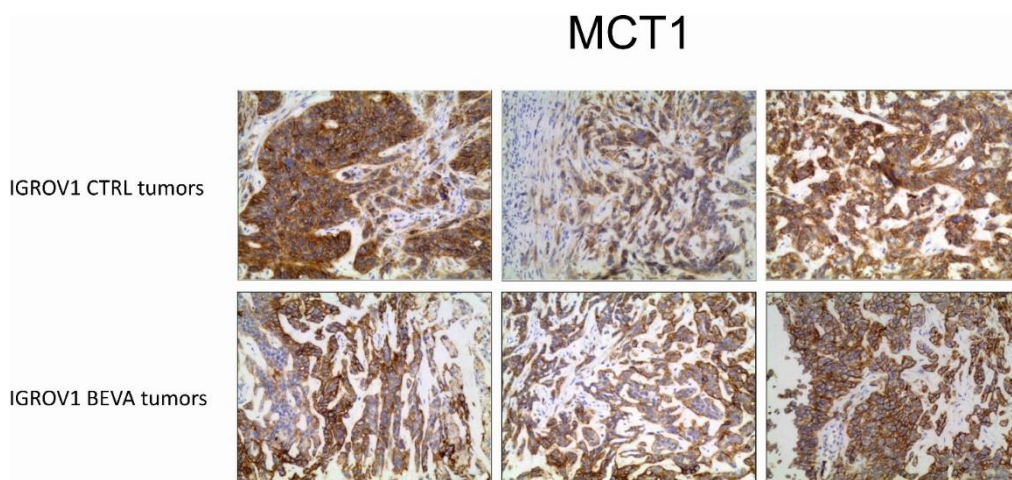

Figure 4.22: Expression of MCT1 in tumor xenografts treated with anti-VEGF mAb or PBS to control group. Immunoreactivity was scored for both the intensity and the proportion of cells staining; intensity was given scores of 0 to 3 (0, no staining; 1,light staining; 2, moderate staining; 3, strong staining) and proportion was given scores of 1 to 6 (1, 0%-4%; 2, 5%-20%; 3, 21%-40%; 4, 41%-60%, 5, 61%-80%; 6, 81%-100%). The scores were multiplied to obtain the final result of 0-18.

Protein lysates obtained from CTRL and BEVA *ex vivo* cultures, were used for protein quantification throught Western Blot. Cells were cultured in P6 plate for 48 h in presence or absence of glucose then cells were collected and lysated for Western Blot. Samples were analyzed for MCT1 and MCT4 proteins. Results showed that MCT1 protein was significant up-regulated in absense of glucose in both groups, whereas MCT4 expression did not substantially change in both groups and conditions.

Notably, MCT1 protein expression was significantly increased in BEVA group compared to CTRL cultures even in the presence or absence of glucose (Figure 4.23). This analysis confirmed the correlation between GDR clones and MCT1 modulation and expression, observed in our previous results.
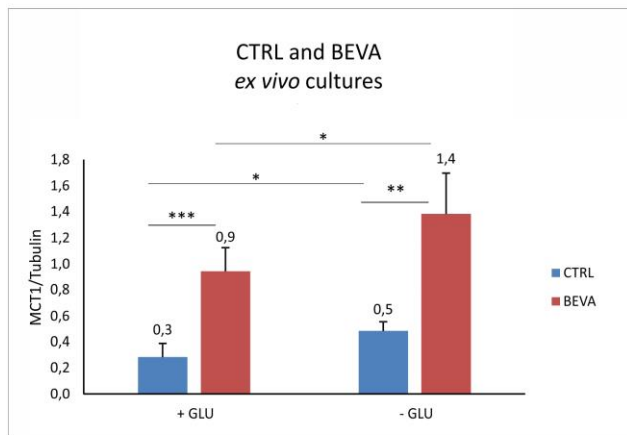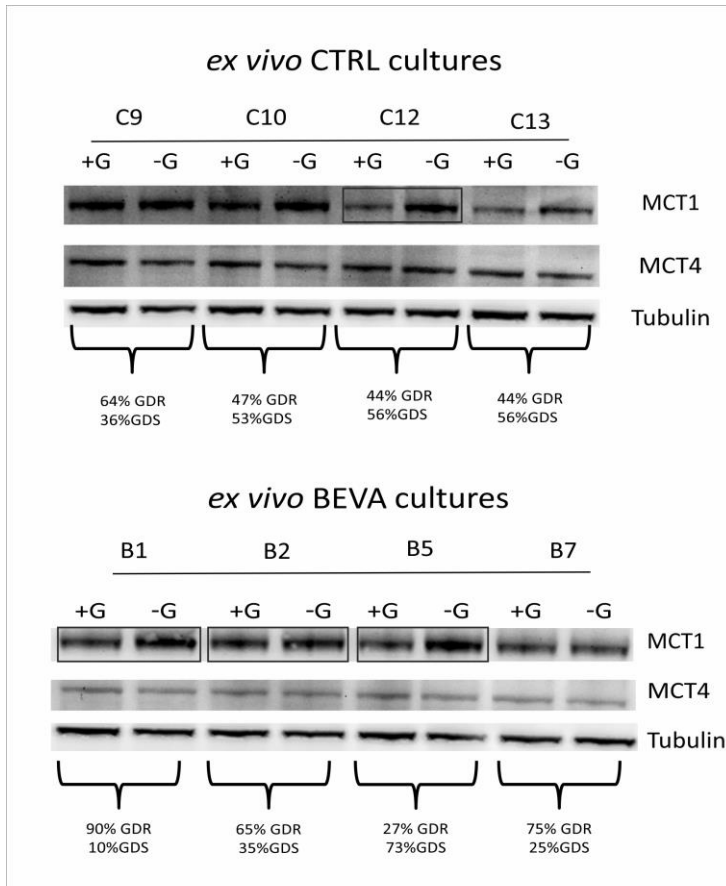
Figure 4.23: MCT1 and MCT4 Western Blot analysis. Western blot analysis of MCT1 and MCT4 transporters in IGROV-1 *ex vivo* control (CTRL) culture and in IGROV-1 *ex vivo* anti-VEGF treated culture (BEVA). In the figure are shown the mean value ± SD of 4 CTRL and 4 BEVA samples with and without glucose, normalized against α-tubulin (*p<0.05; **p<0.01; ***p<0.001). MCT1 protein expression seems up-regulated in 1 of 4 CTRL cultures and in 3 of 4 BEVA cultures under glucose starvation.

5. Discussion

Cancer heterogeneity has been at the heart of much research initiatives in the last ten years, in part due to the increasing availability of novel techniques which enable us to investigate it at various levels (*58, 61*). Although genetic heterogeneity certainly represents the most studied type of cancer heterogeneity, there are many studies which focus on metabolic heterogeneity of tumors (*84, 85*). Most of these studies deal with inter-tumor metabolic heterogeneity, as they describe variations in the metabolic profile of tumors of the same type among different individuals or metabolic differences between the primary tumor and its metastasis. Additional examples include studies on intra-tumor metabolic heterogeneity, which cover regional differences in tumor metabolism in different tumor areas which can also depend from hypoxia or additional perturbations of the tumor microenvironment, such as lack or availability of certain nutrients. Less investigated is the possibility that individual tumor cells might show metabolic heterogeneity. Clearly, certain metabolic differences among tumor cells depend on their proliferative activity. It is well established that actively proliferating cells, including both tumor cells and normal cells, such as lymphocytes, activate certain metabolic processes, including glycolysis, when they turn into proliferation (*86, 87*). Therefore, part of the metabolic differences that one night observe are likely to depend on the resting/proliferative condition of any specific tumor cell or even be related to the specific phase of the cell cycle. Being aware of these facts, we hypothesized that certain metabolic traits could be intrinsic features of tumor cells and we sought to investigate whether this kind of metabolic heterogeneity could exist by analyzing clones derived from one laboratory adapted ovarian cancer cell line. We challenged clones with glucose starvation and found that they exhibit marked inter-clonal heterogeneity in the response to this metabolic stress, which enabled us to classify them into 2 arbitrary categories, namely Glucose Deprivation Resistant (GDR) and Glucose Deprivation Sensitive (GDS) clones.

In our study we isolated GDR and GDS clones from several ovarian cancer cell lines previously characterized from their glycolytic activity. IGROV1 and SKOV3 cells, that are poorly glycolytic cell lines (*88*) had a similar ratio of these clones (50% to 50%), on the other hand, OC316 cells, a highly glycolytic cell line, had only GDS clones (100%). OAW42 were composed by 68% GDR and 32% GDS clones, A2780 and A2774 showed high enrichment in GDR clones. There was no clear-cut correlation between the percentage of GDR/GDS clones found in a particular cell line and its glycolytic activity, measured in terms of lactate production in vitro. We tried to characterize these two types of clones for their metabolic activity. We initially performed Real Time PCR analysis to evaluate expression of several transcripts codifying genes involved in glycolytic pathway, but we did not find any substantial difference between the two types of clones. By Seahorse analysis, we evaluated Oxygen Consumption Rate (OCR) and Extracellular Acidification Rate (ECAR) in different GDR and GDS clones. We observed that GDR clones had higher OCR value compared to GDS clones, whereas baseline ECAR values were comparable. GDS clones may have partially deficient mitochondria activity. Indeed, after Oligomycin administration, GDR clones significant enhanced the ECAR value, whereas GDS clones showed a much milder increase in ECAR. Oligomycin blocked mitochondria activity, therefore enhancing the glycolytic pathway in GDR and GDS clones. GDR clones were more sensitive to this compound compared to GDS clones, this could explain the importance of OXPHOS pathway in GDR clones, especially under glucose starvation. Next, we performed metabolomics analysis that highlighted differences in mitochondria activity in GDR compared to GDS clones. These preliminary results unexpectedly suggested that we could not discriminate GDS clones for their glycolytic activity. Our GDS clones did not show higher glycolytic activity compared to GDR clones but these clones depend on the presence of glucose in the medium. These results are in contrast with previous findings obtained by metabolic characterization of tumor cells selected by being addicted (glucose addicted GA) or not (glucose non-addicted GNA) to glucose. A. Pastò et

al (*76*), reported that GA samples showed a high Warburg effect on the other hand, GNA had a low glycolytic metabolism. In this work they discriminated tumor cells isolated from patients ascitic fluids from 47 carboplatin-treated patients who were categorized as clinically PLT-sensitive or -resistant. They found that in PLT-sensitive samples cell viability dropped upon glucose deprivation instead PLT-resistant displayed lower sensitivity to glucose starvation. By Real-Time PCR, Seahorse analysis and western blot assay they asserted that tumor cells from glucose addicted patients show higher glycolytic activity compared to GNA subjects. On the other hand, GNA patients rely more on autophagy compared to GA patients. They demonstrated that epithelial ovarian cancer cells exhibit heterogeneous glucose addiction and metabolic profiles, and these features strictly correlate with patients response to carboplatin and can in some instances be effected by platinum -based therapy. These contrasting results may depend on the marked differences in the experimental models used in these studies. They described metabolic features of cancer cell cultures derived from patients, but they did not analyze these features at clonal level. Our clones never passed *in vivo* so their metabolic phenotype did not convey the microenvironment or treatment.

Subsequently, we focused our attention in the mitochondria activity that seems modulated in GDR clones. We better characterized this observation with other experiments. We used Metformin, a respiratory chain complex I inhibitor. Metformin decrease mitochondria respiration and reduce glucose metabolism through the citric acid cycle (*89*). We measured that GDR clones seems be more sensitive to this compound compared to GDS, in glucose starvation condition. This result could suggest a mitochondrial pathway dependence of GDR clones but not in GDS clones. From this point, we started with our analysis in glucose starvation culture conditions to enhance the difference between GDR and GDS clones. Trough Real Time PCR and Western Blot analysis we obtained that the intramembrane transporter MCT1 enhance its expression only in GDR clones compared to GDS. This transporter promotes the pyruvate transport inside

mitochondria and the flux of lactate outside the cell (*90*). We tried to test Lonidamine that has been reported as potential MCTs inhibitor. Our experiment suggested that LND had citotoxic effects both in the presence or absence of glucose in GDR and GDS clones. There was no apparent difference between the two groups of clones in the response to LND. This compound had not selective effects on GDR or GDS clones, we can not consider Lonidamina as a potential drug for target GDR clones instead of GDS clones.

In the Figure 5.1 is shown the possible mechanism that help the GDR resistance to glucose starvation. In glucose starvation condition GDR clones enhance MCT1 production. MCT1 transporter could import the extracellular pyruvate that could be used for OXPHOS pathway. On the other hand, GDS seems not enhance the MCT1 expression. Under glucose starvation conditions these clones did not used extracellular pyruvate to promote OXPHOS instead of glycolytic pathway.
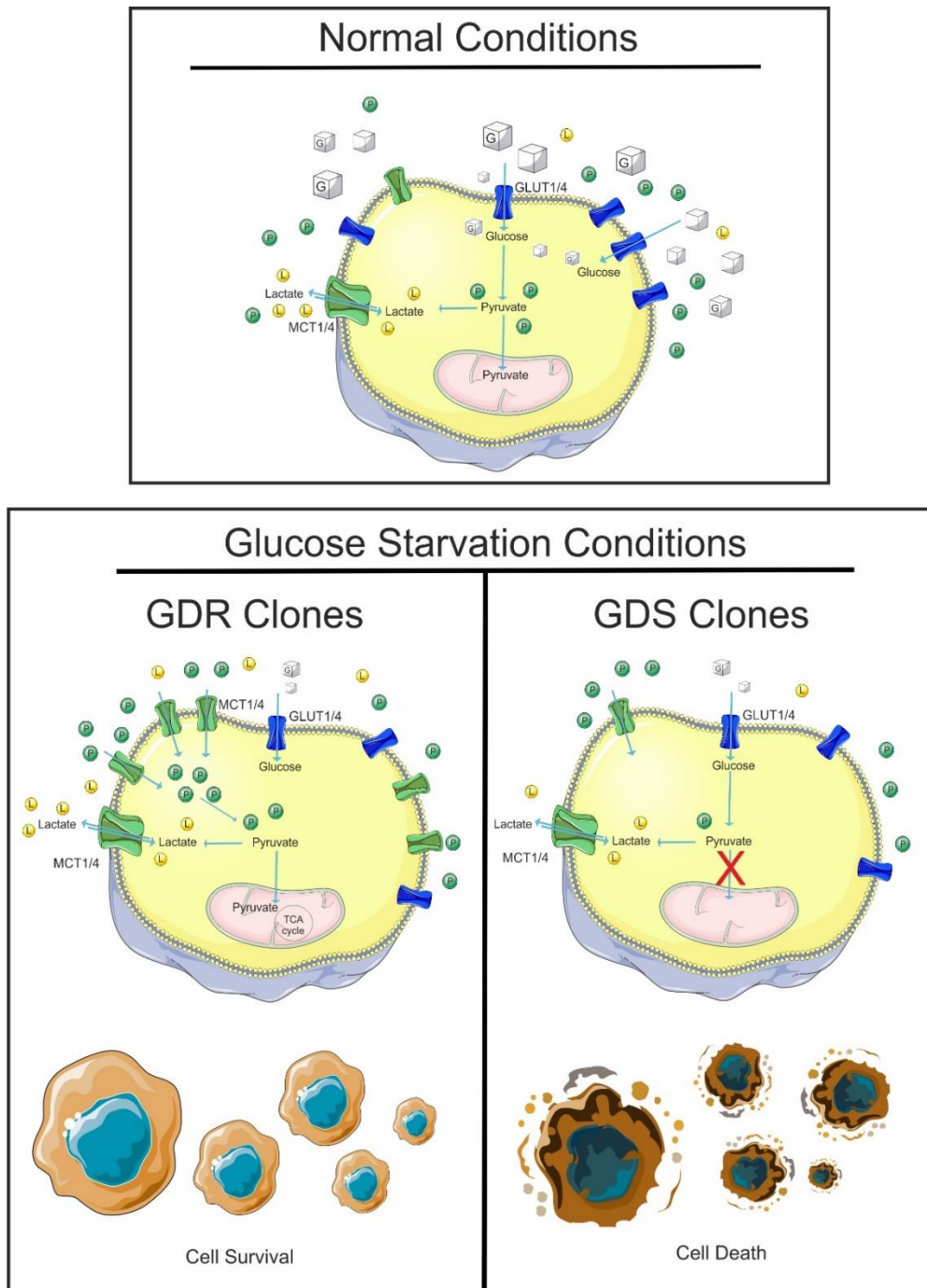
Figure 5.1: possible mechanism highlights GDR resistance to glucose starvation.

GDS clones seems not enhance the mitochondrial activity. By transcriptome and GSEA analysis we confirmed that GDS clones down-regulated the TCA cycle. Analogous results were published in 2014 by Birsoy et al (*75*), they described that the OXPHOS as the major pathway for optimal proliferation in low glucose in their model. Their most sensitive to low glucose cell lines are defective in the

upregulation of OXPHOS normally caused by glucose limitation. Furthermore, because the inhibit mitochondrial metabolism, bioguanides (Metformin, Phenformin) exacerbate the OXPHOS defects of cells sensitive to low glucose, explaining their greater sensitivity to Metformin under low glucose condition. Other published data confirmed that cells cultured in the absence of glucose increased mitochondrial metabolism and were drastically more sensitive to the effects of Metformin than cells grown in the presence of glucose (*89, 91*). Our results were partially in accord with these observations. We found that clones sensitive to glucose starvation showed a deficit in mitochondrial activity compare to clones resistant to glucose starvation, but we did not notice the major sensitivity to Metformin in GDS clones compared to GDR. We observed the exactly contrary, GDR clones were more sensitive to Metformin compared to GDS clones. This could be explained by the different metabolic profile of these clones. GDS clones seems not used OXPHOS pathway in the absence of glucose so they seem not reacts very well to Metformin but in GDR group of clones the result was different. Previously, we speculated that GDR clones had an altered mitochondria pathway compared to GDS clones that seems help these clones to survive under glucose starvation condition. If we used Metformin in this group of clones we perturbed their capacity to survive under glucose starvation condition. Another key finding of our work is the possible modulation of clones ratio in tumors after anti-VEGF treatment.

We studied the metabolic heterogeneity at clonal level to establish whether certain targeted therapies might change tumor metabolism, leading to selection of metabolic variants poorly represented in the original tumor. We characterized GDR and GDS clones subpopulations in control and anti-VEGF treated IGROV-1 *ex vivo* cultures to find how the therapy modulates the metabolic profile and the development of resistance to anti-VEGF therapy. From this analysis, we established that control cultures maintained the parental IGROV-1 cells GDR/GDS clones ratio. On the other hand, anti-VEGF therapy modulates the GDR/GDS clones ratio and seems to increase the GDR clone fraction in 4 of 5 treated

cultures. We aim to investigate the clones ratio in other CTRL and BEVA *ex vivo* cultures. Targeted therapy perturbs the metabolic profile of tumors instead a sub population of resistant clones.

Combined therapy is to be considered important to target the metabolic heterogeneity. For example, Elgogary et al., used Metformin combined with inhibitor of glutamine metabolism (PBTES). Treatment with BPTES resulted in only modest inhibition of tumor growth, in their model, indicating a resistant subpopulation of tumor cells (*92*). But when they combined Metformin with BPTES they observed a greater tumor reduction than with either drug alone. So, these findings emphasized the need to target multiple metabolic pathways to effectively suppress tumor growth. In the final part of our study we noticed that anti-VEGF therapy perturbs the GDR and GDS clones component. The treatment enriched the number of GDR clones in the IGROV-1 ex vivo treated cultures. Previous results, showed that Metformin specifically acts on GDR clones under glucose starvation conditions, so we considered the possibility to used Metformin combined with Bevacizumab *in vivo*, to target GDR clones selected by anti-VEGF therapy.

The resistance to therapy could be described like an adaptation through the concept of "compensatory" metabolism, for example inhibitor targeting glycolysis might trigger metabolic reprogramming toward multiple other pathways (*93*). The GDR and GDS clones are an example of metabolic reprogramming. Perhaps, in the future the analysis of clones component in tumors and the study of their metabolic phenotype, could be used in clinic to choose the specific treatment/inhibitor based on the type of clones that compose the tumor.

6. Bibliography

1. What Is Cancer? - National Cancer Institute. (2007).
2. Cancer statistics, 2018 - Siegel - 2018 - CA: A Cancer Journal for Clinicians - Wiley Online Library. (2018).
3. K. A. Cronin *et al.*, in *Cancer*. (2018), vol. 124, pp. 2785-2800.
4. G. C. o. D. Collaborators, Global, regional, and national age-sex specific mortality for 264 causes of death, 1980-2016: a systematic analysis for the Global Burden of Disease Study 2016. *Lancet* **390**, 1151-1210 (2017).
5. D. Hanahan, R. A. Weinberg, The hallmarks of cancer. *Cell* **100**, 57-70 (2000).
6. D. Hanahan, R. A. Weinberg, Hallmarks of cancer: the next generation. *Cell* **144**, 646-674 (2011).
7. Y. A. Fouad, C. Aanei, Revisiting the hallmarks of cancer. *Am J Cancer Res* **7**, 1016-1036 (2017).
8. Ovarian Epithelial, Fallopian Tube, and Primary Peritoneal Cancer Symptoms, Tests, Prognosis, Stages (PDQ®)—Patient Version - National Cancer Institute. (1980).
9. What Is Ovarian Cancer? , (2018).
10. Ovarian cancer statistics, 2018 - Torre - 2018 - CA: A Cancer Journal for Clinicians - Wiley Online Library. (2018).
11. A. N. Vargas, in *Ecancermedicalscience*. (2014), vol. 8.
12. B. A. Goff, L. S. Mandel, C. H. Melancon, H. G. Muntz, Frequency of symptoms of ovarian cancer in women presenting to primary care clinics. *Jama* **291**, 2705-2712 (2004).
13. M. R. Jones, D. Kamara, B. Y. Karlan, P. D. P. Pharoah, S. A. Gayther, Genetic epidemiology of ovarian cancer and prospects for polygenic risk prediction. *Gynecol Oncol* **147**, 705-713 (2017).
14. N. Wentzensen *et al.*, Ovarian Cancer Risk Factors by Histologic Subtype: An Analysis From the Ovarian Cancer Cohort Consortium. *J Clin Oncol* **34**, 2888-2898 (2016).
15. S. Vos, P. J. van Diest, C. B. Moelans, A systematic review on the frequency of BRCA promoter methylation in breast and ovarian carcinomas of BRCA germline mutation carriers: Mutually exclusive, or not? *Crit Rev Oncol Hematol* **127**, 29-41 (2018).
16. W. Lim, G. Song, Discovery of prognostic factors for diagnosis and treatment of epithelial-derived ovarian cancer from laying hens. *J Cancer Prev* **18**, 209-220 (2013).
17. G. E. Hanley, J. N. McAlpine, J. S. Kwon, G. Mitchell, in *Gynecol Oncol Res Pract*. (2015), vol. 2.
18. J. Prat, FIGO's staging classification for cancer of the ovary, fallopian tube, and peritoneum: abridged republication. *J Gynecol Oncol* **26**, 87-89 (2015).
19. M. McCormack, Radiation Therapy in Ovarian Cancer: An Overview and Future Directions. *Clin Oncol (R Coll Radiol)* **30**, 504-506 (2018).
20. Radiation Therapy for Ovarian Cancer. (2018).
21. C. Gourley, J. L. Walker, H. J. Mackay, Update on Intraperitoneal Chemotherapy for the Treatment of Epithelial Ovarian Cancer. *Am Soc Clin Oncol Educ Book* **35**, 143-151 (2016).

22.   M. Cristea, E. Han, L. Salmon, R. J. Morgan, Practical considerations in ovarian cancer chemotherapy. *Ther Adv Med Oncol* **2**, 175-187 (2010).

23.   D. A. Becker, C. A. Leath, 3rd, C. L. Walters-Haygood, B. Q. Smith, K. S. Bevis, Utilization of an Alternative Docetaxel-based Intraperitoneal Chemotherapy Regimen in Patients With Ovarian, Fallopian Tube or Primary Peritoneal Carcinoma: A Continued Need for Ovarian Cancer Patients. *Am J Clin Oncol*, (2018).

24.   C. Aghajanian *et al.*, OCEANS: a randomized, double-blind, placebo-controlled phase III trial of chemotherapy with or without bevacizumab in patients with platinum-sensitive recurrent epithelial ovarian, primary peritoneal, or fallopian tube cancer. *J Clin Oncol* **30**, 2039-2045 (2012).

25.   E. Pujade-Lauraine *et al.*, Bevacizumab combined with chemotherapy for platinum-resistant recurrent ovarian cancer: The AURELIA open-label randomized phase III trial. *J Clin Oncol* **32**, 1302-1308 (2014).

26.   A. Kim, Y. Ueda, T. Naka, T. Enomoto, Therapeutic strategies in epithelial ovarian cancer. *J Exp Clin Cancer Res* **31**, 14 (2012).

27.   R. Kristeleit *et al.*, A Phase I-II Study of the Oral PARP Inhibitor Rucaparib in Patients with Germline BRCA1/2-Mutated Ovarian Carcinoma or Other Solid Tumors. *Clin Cancer Res* **23**, 4095-4106 (2017).

28.   W. Risau, I. Flamme, Vasculogenesis. *Annu Rev Cell Dev Biol* **11**, 73-91 (1995).

29.   J. Folkman, E. Merler, C. Abernathy, G. Williams, Isolation of a tumor factor responsible for angiogenesis. *J Exp Med* **133**, 275-288 (1971).

30.   A. McIntyre, A. L. Harris, Metabolic and hypoxic adaptation to anti-angiogenic therapy: a target for induced essentiality. *EMBO Mol Med* **7**, 368-379 (2015).

31.   N. S. Vasudev, A. R. Reynolds, Anti-angiogenic therapy for cancer: current progress, unresolved questions and future directions. *Angiogenesis* **17**, 471-494 (2014).

32.   P. Carmeliet, R. K. Jain, Molecular mechanisms and clinical applications of angiogenesis. *Nature* **473**, 298-307 (2011).

33.   Y. Crawford *et al.*, PDGF-C mediates the angiogenic and tumorigenic properties of fibroblasts associated with tumors refractory to anti-VEGF treatment. *Cancer Cell* **15**, 21-34 (2009).

34.   H. P. Gerber, N. Ferrara, Pharmacology and pharmacodynamics of bevacizumab as monotherapy or in combination with cytotoxic therapy in preclinical studies. *Cancer Res* **65**, 671-680 (2005).

35.   R. Leite de Oliveira, A. Hamm, M. Mazzone, Growing tumor vessels: more than one way to skin a cat - implications for angiogenesis targeted cancer therapies. *Mol Aspects Med* **32**, 71-87 (2011).

36.   G. Bergers, D. Hanahan, Modes of resistance to anti-angiogenic therapy. *Nat Rev Cancer* **8**, 592-603 (2008).

37.   S. Giuliano, G. Pages, Mechanisms of resistance to anti-angiogenesis therapies. *Biochimie* **95**, 1110-1119 (2013).

38.   B. Escudier *et al.*, Phase III trial of bevacizumab plus interferon alfa-2a in patients with metastatic renal cell carcinoma (AVOREN): final analysis of overall survival. *J Clin Oncol* **28**, 2144-2150 (2010).

39.   G. Jimenez-Valerio *et al.*, Resistance to Antiangiogenic Therapies by Metabolic Symbiosis in Renal Cell Carcinoma PDX Models and Patients. *Cell Rep* **15**, 1134-1143 (2016).

40. A. J. Montero, M. Escobar, G. Lopes, S. Gluck, C. Vogel, Bevacizumab in the treatment of metastatic breast cancer: friend or foe? *Curr Oncol Rep* **14**, 1-11 (2012).

41. A. de Gramont *et al.*, Bevacizumab plus oxaliplatin-based chemotherapy as adjuvant treatment for colon cancer (AVANT): a phase 3 randomised controlled trial. *Lancet Oncol* **13**, 1225-1233 (2012).

42. L. M. Ellis, D. J. Hicklin, Pathways mediating resistance to vascular endothelial growth factor-targeted therapy. *Clin Cancer Res* **14**, 6371-6375 (2008).

43. J. M. Clarke, H. I. Hurwitz, Understanding and targeting resistance to anti-angiogenic therapies. *J Gastrointest Oncol* **4**, 253-263 (2013).

44. J. Welti, S. Loges, S. Dimmeler, P. Carmeliet, Recent molecular discoveries in angiogenesis and antiangiogenic therapies in cancer. *J Clin Invest* **123**, 3190-3200 (2013).

45. N. Rigamonti *et al.*, Role of angiopoietin-2 in adaptive tumor resistance to VEGF signaling blockade. *Cell Rep* **8**, 696-706 (2014).

46. A. Jahangiri *et al.*, Gene expression profile identifies tyrosine kinase c-Met as a targetable mediator of antiangiogenic therapy resistance. *Clin Cancer Res* **19**, 1773-1783 (2013).

47. J. N. Bottsford-Miller, R. L. Coleman, A. K. Sood, Resistance and escape from antiangiogenesis therapy: clinical implications and future strategies. *J Clin Oncol* **30**, 4026-4034 (2012).

48. K. Kumar *et al.*, Dichloroacetate reverses the hypoxic adaptation to bevacizumab and enhances its antitumor effects in mouse xenografts. *J Mol Med (Berl)* **91**, 749-758 (2013).

49. M. Curtarello *et al.*, VEGF-targeted therapy stably modulates the glycolytic phenotype of tumor cells. *Cancer Res* **75**, 120-133 (2015).

50. P. E. Porporato, S. Dhup, R. K. Dadhich, T. Copetti, P. Sonveaux, Anticancer targets in the glycolytic metabolism of tumors: a comprehensive review. *Front Pharmacol* **2**, 49 (2011).

51. P. Sonveaux *et al.*, Targeting lactate-fueled respiration selectively kills hypoxic tumor cells in mice. *J Clin Invest* **118**, 3930-3942 (2008).

52. E. Allen *et al.*, Metabolic Symbiosis Enables Adaptive Resistance to Anti-angiogenic Therapy that Is Dependent on mTOR Signaling. *Cell Rep* **15**, 1144-1160 (2016).

53. L. Pisarsky *et al.*, Targeting Metabolic Symbiosis to Overcome Resistance to Anti-angiogenic Therapy. *Cell Rep* **15**, 1161-1174 (2016).

54. J. R. Cantor, D. M. Sabatini, Cancer cell metabolism: one hallmark, many faces. *Cancer Discov* **2**, 881-898 (2012).

55. O. Warburg, On the origin of cancer cells. *Science* **123**, 309-314 (1956).

56. R. Moreno-Sanchez, S. Rodriguez-Enriquez, A. Marin-Hernandez, E. Saavedra, Energy metabolism in tumor cells. *FEBS J* **274**, 1393-1418 (2007).

57. G. Gentric, V. Mieulet, F. Mechta-Grigoriou, in *Antioxid Redox Signal*. (2017), vol. 26, pp. 462-485.

58. S. J. Diaz-Cano, Tumor heterogeneity: mechanisms and bases for a reliable application of molecular marker design. *Int J Mol Sci* **13**, 1951-2011 (2012).

59. S. J. Diaz-Cano, Clonality Studies in the Analysis of Adrenal Medullary Proliferations: Application Principles and Limitations. *Endocr Pathol* **9**, 301-316 (1998).

60. L. Pozo-Garcia, S. J. Diaz-Cano, in *Am J Pathol*. (2003), vol. 162, pp. 353-355.

61. D. R. Welch, Tumor Heterogeneity--A 'Contemporary Concept' Founded on Historical Insights and Predictions. *Cancer Res* **76**, 4-6 (2016).

62. G. H. Heppner, Tumor heterogeneity. *Cancer Res* **44**, 2259-2265 (1984).

63. A. Skibinski, C. Kuperwasser, The origin of breast tumor heterogeneity. *Oncogene* **34**, 5309-5316 (2015).

64. S. Huang, Genetic and non-genetic instability in tumor progression: link between the fitness landscape and the epigenetic landscape of cancer cells. *Cancer Metastasis Rev* **32**, 423-448 (2013).

65. P. Valent *et al.*, Heterogeneity of neoplastic stem cells: theoretical, functional, and clinical implications. *Cancer Res* **73**, 1037-1045 (2013).

66. J. A. Magee, E. Piskounova, S. J. Morrison, Cancer stem cells: impact, heterogeneity, and uncertainty. *Cancer Cell* **21**, 283-296 (2012).

67. C. A. Klein, Selection and adaptation during metastatic cancer progression. *Nature* **501**, 365-372 (2013).

68. L. A. Loeb, J. H. Bielas, R. A. Beckman, Cancers exhibit a mutator phenotype: clinical implications. *Cancer Res* **68**, 3551-3557; discussion 3557 (2008).

69. L. A. Loeb, Human cancers express mutator phenotypes: origin, consequences and targeting. *Nat Rev Cancer* **11**, 450-457 (2011).

70. M. Greaves, C. C. Maley, Clonal evolution in cancer. *Nature* **481**, 306-313 (2012).

71. I. Dagogo-Jack, A. T. Shaw, Tumour heterogeneity and resistance to cancer therapies. *Nat Rev Clin Oncol* **15**, 81-94 (2018).

72. P. C. Nowell, The clonal evolution of tumor cell populations. *Science* **194**, 23-28 (1976).

73. L. M. Merlo, J. W. Pepper, B. J. Reid, C. C. Maley, Cancer as an evolutionary and ecological process. *Nat Rev Cancer* **6**, 924-935 (2006).

74. J. W. Pepper, C. Scott Findlay, R. Kassen, S. L. Spencer, C. C. Maley, Cancer research meets evolutionary biology. *Evol Appl* **2**, 62-70 (2009).

75. K. Birsoy *et al.*, Metabolic determinants of cancer cell sensitivity to glucose limitation and biguanides. *Nature* **508**, 108-112 (2014).

76. A. Pasto *et al.*, Resistance to glucose starvation as metabolic trait of platinum-resistant human epithelial ovarian cancer cells. *Oncotarget* **8**, 6433-6445 (2017).

77. J. H. Hung, T. H. Yang, Z. Hu, Z. Weng, C. DeLisi, in *Brief Bioinform*. (2012), vol. 13, pp. 281-291.

78. P. L. Lorenzi *et al.*, DNA fingerprinting of the NCI-60 cell line panel. *Mol Cancer Ther* **8**, 713-724 (2009).

79. F. Del Ben *et al.*, A Method for Detecting Circulating Tumor Cells Based on the Measurement of Single-Cell Metabolism in Droplet-Based Microfluidics. *Angew Chem Int Ed Engl* **55**, 8581-8584 (2016).

80. L. R. Gray, S. C. Tompkins, E. B. Taylor, Regulation of pyruvate metabolism and human disease. *Cell Mol Life Sci* **71**, 2577-2604 (2014).

81. C. S. Hong *et al.*, MCT1 modulates cancer cell pyruvate export and growth of tumors that co-express MCT1 and MCT4. *Cell Rep* **14**, 1590-1601 (2016).

82. B. Nancolas *et al.*, The anti-tumour agent lonidamine is a potent inhibitor of the mitochondrial pyruvate carrier and plasma membrane monocarboxylate transporters. *Biochem J* **473**, 929-936 (2016).

83. O. Casanovas, D. J. Hicklin, G. Bergers, D. Hanahan, Drug resistance by evasion of antiangiogenic targeting of VEGF signaling in late-stage pancreatic islet tumors. *Cancer Cell* **8**, 299-309 (2005).

84. M. Robertson-Tessi, R. J. Gillies, R. A. Gatenby, A. R. Anderson, Impact of metabolic heterogeneity on tumor growth, invasion, and treatment outcomes. *Cancer Res* **75**, 1567-1579 (2015).

85. L. K. Boroughs, R. J. DeBerardinis, Metabolic pathways promoting cancer cell survival and growth. *Nat Cell Biol* **17**, 351-359 (2015).

86. K. A. Frauwirth, C. B. Thompson, Regulation of T lymphocyte metabolism. *J Immunol* **172**, 4661-4665 (2004).

87. W. Palm, C. B. Thompson, Nutrient acquisition strategies of mammalian cells. *Nature* **546**, 234-242 (2017).

88. G. Nardo *et al.*, Glycolytic phenotype and AMP kinase modify the pathologic response of tumor xenografts to VEGF neutralization. *Cancer Res* **71**, 4214-4225 (2011).

89. S. Andrzejewski, S. P. Gravel, M. Pollak, J. St-Pierre, Metformin directly acts on mitochondria to alter cellular bioenergetics. *Cancer Metab* **2**, 12 (2014).

90. I. Marchiq, R. Le Floch, D. Roux, M. P. Simon, J. Pouyssegur, Genetic disruption of lactate/H+ symporters (MCTs) and their subunit CD147/BASIGIN sensitizes glycolytic tumor cells to phenformin. *Cancer Res* **75**, 171-180 (2015).

91. S. Javeshghani *et al.*, Carbon source and myc expression influence the antiproliferative actions of metformin. *Cancer Res* **72**, 6257-6267 (2012).

92. A. Elgogary *et al.*, Combination therapy with BPTES nanoparticles and metformin targets the metabolic heterogeneity of pancreatic cancer. *Proc Natl Acad Sci U S A* **113**, E5328-5336 (2016).

93. M. L. Avantaggiati, Cancer metabolism as a therapeutic target: finding the right target(s) in the context of tumor heterogeneity, evolution, and metabolic plasticity. *Oncology (Williston Park)* **27**, 474, 476-477 (2013).